Psychobiophysics of Transcranial Magnetic Stimulation

Thesis by

Yukiyasu Kamitani

In Partial Fulfillment of the Requirements

for the Degree of

Doctor of Philosophy

California Institute of Technology

Pasadena, California

2001

(Defended March 21, 2001)

Acknowledgements

The work for this thesis was carried out in the Psychophysics Laboratory at California Institute of Technology. The advisor of the work was Prof. Shinsuke Shimojo. I am grateful for his invaluable support. I also want to thank the members of my thesis committee: Prof. Gilles Laurent, Christof Koch, Masakazu Konishi, and Richard Andersen.

All of the work was collaboration with Prof. Shimojo. Part of it was carried out with Yoshi-hisa Kubota, Vidya Bhalodia, and Daw-An Wu. I would like to express my gratitude to the collaborators. When I started experimental work using TMS, I learned basics of the technique from Yoshikazu Ugawa, Yasuo Terao, and Ritsuko Hanajima at University of Tokyo. Prof. Koch and Amit Manwani helped me start the modeling project. Also, Michael Hines and Zachary Mainen responded to my inquiry concerning compartmental models, and provided me with part of the codes used in my simulation. I thank all these people who supported my work. I wish to express my gratitude to Daw-An Wu, Fumiko Maeda, Yoshi-hisa Kubota, and Prof. Shimojo for reviewing the manuscript of this thesis. While I was writing this thesis, Ladan Shams gave me patient encouragement which I greatly valued. I am also grateful to the people in the Psychophysics Laboratory for their helpful comments and discussion on my work. Finally, I thank my parents for their support, understanding, and encouragement, which enabled me to pursue science.

Some of the material in this thesis is used with permission from the copyright owners: Nature America Inc. (Nature Neuroscience), Elsevier Science (Neurocomputing), and Cambridge University Press (Journal of Physiology).

This work was financially supported by Caltech Engineering Research Center NSF grant (#EEC-9402726) and anonymous donation for our project (SS4.00003-1-GIFT.000022).

Abstract

Transcranial magnetic stimulation (TMS) is a technique that stimulates the brain using a magnetic coil placed on the scalp. Since it is applicable to humans non-invasively, directly interfering with neural electrical activity, it is potentially a good tool to study the direct relationship between perceptual experience and neural activity. However, it has been difficult to produce a clear perceptible phenomenon with TMS of sensory areas, especially using a single magnetic pulse. Also, the biophysical mechanisms of magnetic stimulation of single neurons have been poorly understood.

In the psychophysical part of this thesis, perceptual phenomena induced by TMS of the human visual cortex are demonstrated as results of the interactions with visual inputs. We first introduce a method to create a hole, or a scotoma, in a flashed, large-field visual pattern using single-pulse TMS. Spatial aspects of the interactions are explored using the distortion effect of the scotoma depending on the visual pattern, which can be luminance-defined or illusory. Its similarity to the distortion of afterimages is also discussed. Temporal interactions are demonstrated in the filling-in of the scotoma with temporally adjacent visual features, as well as in the effective suppression of transient visual features. Also, paired-pulse TMS is shown to lead to different brightness modulations in transient and sustained visual stimuli.

In the biophysical part, we first develop a biophysical theory to simulate the effect of magnetic stimulation on arbitrary neuronal structure. Computer simulations are performed on cortical neuron models with realistic structure and channels, combined with the current injection that simulates magnetic stimulation. The simulation results account for general and basic characteristics of the macroscopic effects of TMS including our psychophysical findings, such as a long inhibitory effect, dependence on the background activity, and dependence on the direction of the induced electric field.

The perceptual effects and the cortical neuron model presented here provide foundations for the study of the relationship between perception and neural activity. Further insights would be obtained from extension of our model to neuronal networks and psychophysical studies based on predictions of the biophysical model.

Contents

List of Figures

Chapter 1 Introduction

There has been explosive growth in the development and use of non-invasive tools for the study of the human brain in recent years. Human brain functions have been revealed by measuring electromagnetic magnetic fields, metabolism, or hemodynamics of the brain using electroenchephalography (EEG), magnetoencephalography (MEG), positron emission tomography (PET), or functional magnetic resonance imaging (fMRI). One of the major interests driving the development and use of these techniques is in the relationship between brain activity and subjective aspects of human experience such as perceptual awareness, which is difficult to study using animal models.

This thesis is concerned with another non-invasive method, transcranial magnetic stimulation (TMS; for overview, see Chokroverty (1989), Ueno, (1994), and Hallet (2000)). It exerts its effects through a coil placed on the scalp which generates single or multiple magnetic pulses (Figure 1.1). Since biological tissue is nearly transparent to magnetic fields, the field penetrates into the cerebral cortex with little loss, inducing an electric field according to its changing rate (Faraday's law). The induced electric field in turn interferes with neural electrical activity, exciting or disrupting brain functions. While TMS modifies neural activity that in turn changes a mental or behavioral state, brain imaging techniques, such as PET and fMRI, measure neural responses, given an experimentally controlled mental or behavioral state. Hence, TMS is complementary to the imaging techniques in establishing the brain-mind relationship.

Since TMS is non-invasively applicable to the human brain, interfering directly with neural electrical activity such as ionic currents and membrane potentials, it is potentially a powerful tool to study the detailed relationship between conscious perceptual experience and neural electrical activity. Because of the direct causality, TMS achieves great temporal precision on the order of 10-100 ms in affecting human behavior and cognition. In this regard, TMS can be contrasted with PET and fMRI, which are mediated by non-electrical physiological states, and thus have only limited temporal resolution on the order of seconds.

However, we have been confronted by two fundamental difficulties in investigating the connections between perception and neural activity using TMS. First, whereas the motor

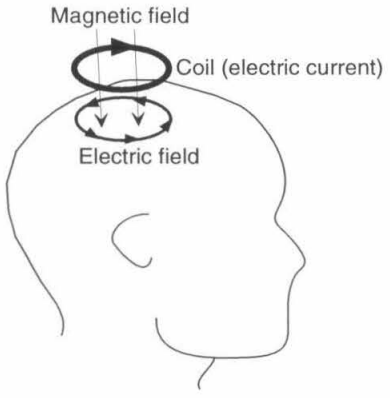

Figure 1.1: Basic principle of TMS
The current in the coil placed on the scalp generates a magnetic field, which in turn induces an electric field. The induced electric field interferes with neural electrical activity in the brain.

area can be easily stimulated to elicit muscle twitches, it has been difficult to produce clearly perceptible effects with TMS of sensory cortical areas, especially with a single magnetic pulse. Second, in spite of numerous reports on the effects of TMS at the behavioral level, the biophysical mechanisms of magnetic stimulation of single cortical neurons are largely unknown.

In an attempt to bridge the gap between perception and neural activity using TMS, this thesis deals with two different levels of systems neuroscience: psychophysics of human visual perception, and biophysics of single cortical neurons. In Part I, the effects of TMS on the human visual cortex are made directly and explicitly perceptible as results of the interactions with visual stimuli. In Part II, biophysical theory and computer simulation are developed to elucidate the mechanisms of magnetic stimulation of single cortical neurons, while referring to the relation to perceptual and behavioral effects of TMS, including those presented in Part I. The last chapter summarizes and discusses the overall findings. The results presented in this thesis are separately published, or in preparation for publication (Kamitani & Shimojo, 1998; Shimojo & Kamitani, 1998; Kamitani, Shimojo & Takahashi, 1998; Kamitani & Shimojo, 1999a,b; Shimojo & Kamitani, 1999; Wu, Kamitani, Maeda & Shimojo, 2001; Kamitani, Bhalodia, Kubota & Shimojo, in press).

Part I

Psychophysics (Chapter 2–5)

Chapter 2 Magnetic stimulation of the human brain: An overview

2.1 History of non-invasive magnetic stimulation

d'Arsonval (1896) reported the first attempt of non-invasive magnetic stimulation of the human brain. He placed the head of a human subject inside a large magnetic coil, and applied electric currents into the coil to induce a time-varying magnetic field. The subjects experienced phosphenes (perception of bright fields) and vertigo, as well as syncope in some cases. The phenomenon of phosphenes was later replicated by many scientists, but is now believed to be caused by the stimulation of the retina, rather than the brain (Dunlap, 1911; Magnusson & Stevens, 1911; Walsh, 1946; Barlow *et al.*, 1947). The changing rate of the magnetic field used in the early studies may have been too low to elicit brain stimulation.

Barker *et al.* (1985) achieved the first successful magnetic stimulation of the human brain based on the technique used in the magnetic stimulators for peripheral nerves developed by Hallgren (1973) and Polson *et al.* (1982). They used a short magnetic pulse produced by discharging a charged capacitor into the coil. The charge-discharge circuitry permitted the delivery of stimuli with a high frequency and changing rate. They reported that the stimulation over the human motor cortex caused twitches in hand muscles about 25 ms after the magnetic stimulation. It was also shown that TMS caused little pain: the subject usually felt only a not uncomfortable sensation of scalp being pinched. This is a significant advantage over transcranial electrical stimulation (TES; Merton & Morton, 1980), which delivers strong currents to scalp electrodes, causing great pain.

The technology of magnetic stimulators has remained mostly unchanged since 1985. However, there have been developments in the design of the coil. While circular coils have been widely used, coils with complex geometry such as figure-of-eight coils (Ueno *et al.*, 1988) and slinky coils (Ren *et al.*, 1995) are now available. These coils were designed for better focality or energy efficiency. Another important technical advance is the development of repetitive stimulators. They can deliver trains of magnetic pulses of 1-50 Hz (repetitive

TMS or rTMS), while conventional stimulators are able to produce only one pulse every several seconds.

2.2 Standard setup for human brain stimulation

Magnetic stimulation of the human brain has been carried out generally using a circular or figure-of-eight magnetic coil with a diameter of 5-12 cm, which generates a brief magnetic pulse of about 1 ms duration with a peak magnetic field of 1.2-2.2 Tesla (see Chapter 6 for physics of magnetic stimulation). The coil is placed on the subject's scalp such that a cortical area of interest falls below a part of the winding of a circular coil, or the intersection of two loops of a figure-of-eight coil, where the strength of the induced electric field is maximum. The electric field is generated parallel to the surface of the coil with a monotonically decreasing strength as a function of the distance from the coil surface. Therefore, the cortical areas, rather than subcortical areas, are believed to be primary sites of stimulation (Epstein *et al.*, 1990; Rudiak and Marg, 1994). The electric field spatially extends over a few centimeters at half amplitudes, though the actual cortical area being stimulated is difficult to define. The spatial resolution should depend on cortical anatomy such as the folding pattern, as well as the biophysical mechanisms of magnetic stimulation of cortical neurons, which have been largely unknown (see Part II).

2.3 Application to cortical areas

Single magnetic pulses, which are believed to leave little lasting effect and to be safe, have been commonly used to activate or disrupt cortical functions. The human motor cortex can be stimulated to produce motor evoked potentials in muscles and to interfere with voluntary movements (Mills, 1991, Rothwell, 1993; Day *et al.*, 1989; Pascual-Leone *et al.*, 1992). However, it is generally difficult to observe prominent effects with single pulses applied over sensory areas, though the disruption of perceptual performances have been reported for the somatosensory and visual areas (Cohen *et al.*, 1991; Amassian *et al.*,1989). rTMS is now available to produce greater effects than single pulses, such as the disruption of speech (Pascual-Leone *el al.*, 1991), or to induce long lasting facilitation or inhibition (Pascual-Leone *el al.*, 1999). rTMS has the potential to cause seizures even in normal

humans. Safety guidelines have been published to prevent such problems (Wasserman, 1998).

The visual cortex has been studied mainly using single-pulse TMS (for review, see Amassian *et al.* (1998)). Documented effects are generally suppressive (Amassian *et al.*, 1989; Beckers & Hömberg, 1992; Epstein *et al.*, 1996), though a small number of studies reported phosphenes (Meyer *et al.*, 1991; Marg & Rudiak, 1994; Kastner *et al.*, 1998). Suppression is typically characterized by deteriorated performance in discrimination or identification tasks that use briefly presented, small visual targets such as letters followed by a single magnetic pulse. Even though the task performance clearly indicates suppressive effects, it is difficult to directly "perceive" them as spatial or temporal interruption of aspects of visual perception in a single trial of TMS, especially while viewing a stationary scene. If the range and characteristics of the suppression could be identified in a single instance of perception, it would allow us to study the relationship between human perception and neural electrical activity more directly and in greater detail than previously possible.

2.4 Visual perception induced by TMS: A perspective

In the following chapters of Part I, we demonstrate directly perceptible effects of TMS as results of the interactions with visual inputs. In Chapter 3, we introduce a method allowing visualization of the suppression as a region of visual space missing a pattern in a flashed, large-field visual stimulus. In Chapter 4, spatial interactions of magnetic and visual stimulation will be explored by observing the shape of the scotoma perceived on various spatial patterns. Also, the similarity with afterimages projected on the visual patterns will be discussed. Chapter 5 characterizes temporal aspects of the interactions by perceptual filling-in of scotomas with temporally adjacent visual features, as well as by the effects of TMS on various temporal phases of a small visual target presented within the scotoma region. We also briefly discuss the interaction between visual stimuli and paired-pulse TMS, which has been recently reported to produce phosphenes reliably (Boroojerdi *et al.*, 2000).

2.5 General experimental methods

Here, general methods for our psychophysical experiments are provided. The details of experimental procedure will be described for each experiment in the succeeding chapters.

2.5.1 Magnetic stimulation

A Magstim Model 200 magnetic stimulator with a 70-mm double (figure-of-eight) coil (Magstim Company, Wales, UK) was used (2.2 T maximum output at the coil surface; monophasic pulse; duration, 1 ms; rise time, 100 μs). The coil location was defined relative to the inion (external occipital protuberance of the skull). The power was adjusted to a value slightly above the threshold of each subject to observe effective suppression as measured by the scotoma procedure described in the following chapter (70-90% maximum output). Paired-pulse stimulation was achieved by combining two Magstim Model 200 units using the Bistim Module (Magstim Company), which allowed the output currents from the two stimulators to flow into a single coil. For some of the preliminary observations and experiments, a NEOPULSE stimulator (Neotonus, GA, USA) was used. The use of TMS was approved by the human subject internal review board at California Institute of Technology.

2.5.2 Visual stimuli

Visual stimuli were presented on a CRT monitor (Sony Multiscan20seII) with a frame rate of 75 Hz, and controlled by a personal computer (Apple Power Macintosh 7600 or 9500). The computer also controlled the timing of magnetic stimulation relative to the visual stimuli through an I/O board (National Instruments PCI-MIO E). The observation distance was 57 cm, and experiments were conducted in a semi-dark room.

2.5.3 Subjects

All subjects had normal or corrected-to-normal visual acuity. We confirmed that they had never suffered from neurological diseases to avoid possible risks due to TMS. A different number of subjects participated in each experiment (three to seven). In each experiment, there was at least one subject who was not aware of the purpose. The number of subjects will be indicated in the corresponding result. The subjects of the experiments using single

magnetic pulses did not perceive phosphenes when TMS was applied without visual stimuli. Informed consent was obtained from all subjects.

Chapter 3 TMS-induced scotomas

3.1 Basic phenomenon

We first explored a method with which the spatial extent of suppression induced by single-pulse TMS could be directly perceived. We reasoned that, if TMS interferes with neural signals projecting onto a limited area of the cortical retinotopic representation, the TMS-induced suppression should be perceived as a gap in pattern vision with a large-field, patterned stimulus.

To test this hypothesis, we presented a large disk (diameter, $>$ 13 deg) with a grid pattern consisting of vertical and horizontal gratings of 50% contrast (mean luminance, 22.3 cd/m^2; 0.45-3.0 cycles/deg, typically 1.5 cycles/deg) on a gray background for 40 ms instead of a small target as commonly used in previous studies (Amassian *et al.*, 1989; Beckers & Hömberg, 1992; Epstein *et al.*, 1996). A single magnetic pulse was applied with a delay of about 100 ms after the onset of the visual stimulus (Figure 3.1a). This delay is known to be effective for the suppression of small visual targets (Amassian *et al.*, 1989). The coil was eight-shaped, and its center (the intersection of the two windings) was placed a few centimeters lateral to and above the inion (Figure 3.1b). The coil was oriented to induce an electric field at 45 deg in the left hemisphere and 135 deg in the right (upward and toward the midline) to optimize the effect (Amassian *et al.*, 1994). During the trial, the subject was asked to fix the gaze on a fixation point displayed in the center of the screen.

Under these conditions, the majority of the observers preliminarily tested reported that the briefly presented, patterned stimulus appeared with a patch missing from the grid pattern in the lower quadrant of the visual field contralateral to the coil position (Figure 3.1c). The region generally appeared homogeneous and gray, though some observers reported that it was slightly colored.

Stimulation at scalp locations other than the occipital lobe, such as the frontal or temporal lobes, did not produce such percept, but often elicited blinks and eye movements leading to general suppression of visual responses. The local homogeneous region was not created in a steadily shown pattern, though longer durations of the flash (up to 100 ms) led

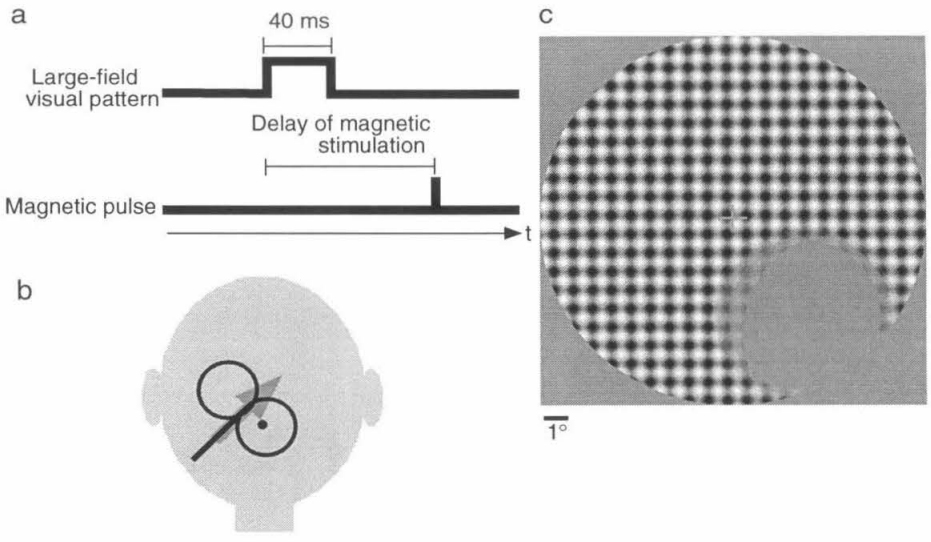

Figure 3.1: TMS-induced scotomas
(a) Time course of a large-field patterned stimulus and magnetic stimulation. The duration of magnetic stimulation was less than 1 ms. The delay of magnetic stimulation refers to the time from the onset of the visual stimulus to that of the magnetic stimulation. (b) Coil placement. A figure-of-eight coil and the back of a head are schematically illustrated. The inion is indicated by the filled dot. The arrow represents the major component of the induced electric field. The coil was oriented at 45 deg in the left hemisphere and 135 deg in the right (upward and toward the midline). (c) Reconstructed percept obtained from a subject.

to a similar effect. Note also that although most observers did not see phosphenes when a magnetic pulse was applied alone, they nevertheless reported the homogeneous region in the flashed pattern. Hence, the region missing the pattern seems to be the direct visualization of the suppressive effect of TMS on the visual cortex. We hereafter refer to the local suppression as a TMS-induced scotoma. When a large homogeneous disk was flashed instead of a grid pattern, a similar "hole" was observed in it. However, since the border of the suppressed region was clearer in patterned disks than in homogeneous disks, we mostly used patterned visual stimuli to observe the scotoma.

3.2 Measuring and reconstructing scotomas

Data on the scotoma was collected in the following manner. After the visual stimulus was flashed and followed by a magnetic pulse, the visual stimulus appeared again on the screen. Using a computer mouse, the subject drew an ellipse on the screen to match the region missing the pattern; if the suppressed region was not observed, the subject indicated this by clicking the mouse. In drawing the ellipse, the subject adjusted the position and the lengths of the horizontal and vertical axes. These small number of parameters adequately represented the percept, as observers usually reported the suppressed region not to be dented, angular, or very obliquely oriented. Five trials were repeated for any given condition. In catch trials, ineffective delays (0 or 40 ms delay) were used as a control for false alarms or cognitive artifacts. In most of these trials, subjects reported the absence of a scotoma.

The data of the five repeated trials were converted to a reconstructed percept as shown in Figure 3.1c. For each pixel, the ratio of trials where the pixel was included in the elliptical suppressed region was calculated. Contrast of the pattern was then modulated by $(1 - \langle ratio\ of\ suppression \rangle)$. Thus, the region included in the ellipses in most trials looks homogeneous, whereas the region mostly outside the ellipses has higher contrast. This transformation of the original data allows us to visualize approximately what the subject perceived and to assess its consistency over trials.

The reconstruction shown in Figure 3.1c was obtained from a subject when a grid pattern (0.9 cycles/deg; diameter, 21 deg) was presented, followed by a magnetic pulse delivered by an eight-shaped coil placed on the left occipital lobe (2 cm left of and above the inion), with a delay of 106 ms. Note that this subject tended to perceive a larger scotoma centered

in the periphery, compared to other subjects. The size of the suppressed region varied substantially across eight subjects studied under similar conditions, the longer axis of the scotoma ranging from 1.2 to 5.6 deg. Anatomical variability in orientation and proximity of the cortex to the scalp (Stensaas *et al.*, 1974) may contribute to such differences.

3.3 Time course

The relative timing between the flashing of a small visual target and TMS has been known to be critical for the suppression of the visual performance (Amassian *et al.*, 1989; Amassian *et al.*, 1993). The effective timing for suppression, typically a delay of 100 ms from the visual stimulus to the magnetic pulse, is thought to reflect the time course of afferent signals reaching the visual cortex. The delay of 100 ms is consistent with the latency for one of the major peaks (P100) in human visual evoked potentials (VEP) (Halliday, 1982).

To see whether the scotoma shows a similar dependency on timing, the delay of the magnetic stimulation from the onset of the visual pattern was varied (40-200ms; 13.3 ms step; randomized order). The spatial frequency of the pattern was also manipulated (0.45, 0.9, or 1.8 cycles/deg), since different spatial frequency components are known to take different time courses in visual processing (Tolhurst, 1975; Breitmeyer & Ganz, 1976).

In Figure 3.2, the mean size of the scotoma (relative to the disk size) for a representative subject is plotted as a function of the delay of magnetic stimulation, for different spatial frequencies. Other four subjects showed similar results. The effective delay for the suppression ranged from 60 to 180 ms peaking at 80-120 ms, roughly in agreement with the previous research using small letters (Amassian *et al.*, 1989). Furthermore, the peak in the size of the scotoma shifts to longer delays as the spatial frequency increases. This is consistent with the idea that higher spatial frequency components are processed more slowly than lower frequency components, which has been supported by reaction time (Breitmeyer, 1975) and VEP (Parker, 1977) studies.

Another important point to note is that the size of the scotoma changed rather abruptly with the delay of the magnetic stimulation: in most trials, the scotoma was either nearly fully visible or invisible (and not inbetween). The same abrupt change in size was observed also when the intensity of magnetic stimulation was gradually changed: the scotoma suddenly began to appear with a large size as the intensity was increased. These suggest highly

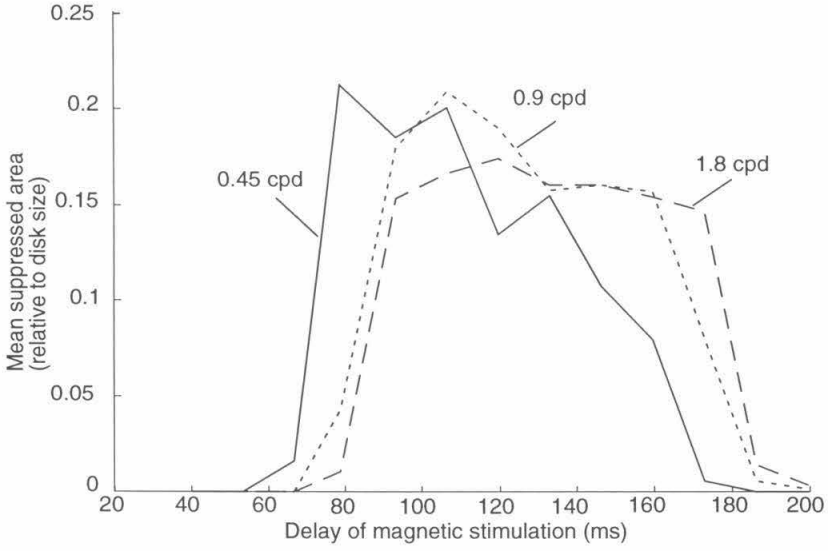

Figure 3.2: Time course of TMS-induced scotomas
The mean suppressed (relative to the disk size) area for a subject is plotted as a function of the delay of magnetic stimulation for different spatial frequencies of the grid pattern.

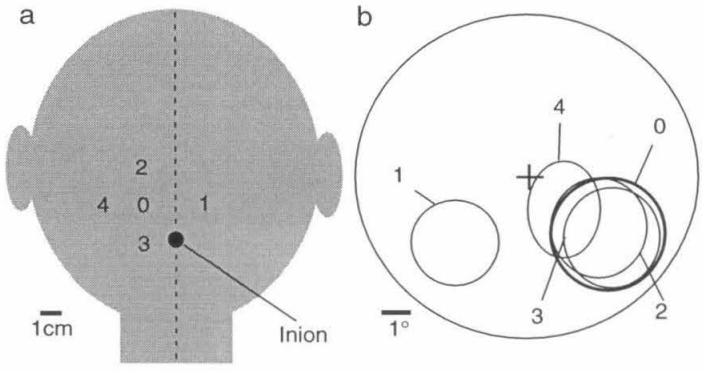

Figure 3.3: Spatial mapping
(a) Positions of the center of the coil. The center of the coil was shifted from the base position (**0**, 2 cm left of above the inion) to the contralateral, symmetrical position (1), to the upper and lower positions by 2 cm (**2**, **3**), and to the lateral position by 2 cm (**4**). (b) Scotomas for the different coil positions. Each ellipse represents the mean position and the mean lengths of the axes of the ellipses drawn by for a subject.

nonlinear machanisms underlying the TMS-induced scotoma.

3.4 Spatial mapping

To further validate our technique, we shifted the coil position and compared the results with the known anatomy of visual cortex (Figure 3.3). The coil location was varied by 1-2 cm around the inion, while the delay of magnetic stimulation (106 ms) and the visual pattern (a grid of 1.5 cycles/deg) were fixed. Note that this technique allows determination of a suppressed region with high resolution with only a single trial, whereas many trials are required for characterization based on performance in discriminating or identifying small visual targets at various locations (Amassian *et al.*, 1989; Epstein *et al.*, 1996; Kastner *et al.*, 1998).

Figure 3.3a and b show the locations of the coil center and the corresponding scotomas (the mean location and size), respectively, for a representative subject (among six). When the coil was shifted to the contralateral, symmetrically positioned spot (**0** to **1** in Figure 3.3a), the scotoma moved to the contralateral visual field as in previous TMS studies (Amassian *et al.*, 1989; Epstein *et al.*, 1996; Kastner *et al.*, 1998). The suppressed location

did not change significantly with changes in the vertical coil position (**0**, **2** and **3**), and suppression was rarely perceived in the upper visual field (Epstein *et al.*, 1996; Kastner *et al.*, 1998). This may be because lower portions of the visual cortex representing the upper visual field are further from the scalp as observed in MRI images. The lateral shift within the hemisphere (**0** to **4**) increased foveal suppression, consistent with the anatomy in that the map of the foveal visual field is located in superficial regions of cortex and extends laterally (Horton & Hoyt, 1991).

In general agreement with previous studies, these results confirmed that the visualized suppressed region indeed reflected interference of TMS with the activity of the cortical retinotopic representation, rather than an artifact caused by muscular contraction or the sound generated by the coil. The effect of laterally shifting the TMS site within the hemisphere, however, had not been previously found. The exact cortical site of stimulation is unclear (V1, V2/V3 or both); it might be possible to identify this site by combining location of the scotoma with a cortical retinotopic map obtained with fMRI (Sereno *et al.*, 1995; DeYoe *et al.*, 1996) for each subject.

3.5 Direction of electric field

Amassian *et al.* (1994) demonstrated that the visual field in which a visual target is inhibited depends on the direction of the induced electric field in the occipital lobe. They changed the direction by flipping the sides of a circular coil at the same location. It was shown that when the direction of the induced electric field is leftward (rightward), a visual target presented in the left (right) visual field was likely to be inhibited. Thus, an electric field to the left (right) seems to interfere with the right (left) cortical area: in other words, an electric field toward the midline is effective for the suppression of the visual cortex.

To confirm the dependency on the electric field direction with our paradigm, the scotoma was measured, while the figure-of-eight coil was centered on the occipital midline and the direction of the electric field was changed (leftward or rightward) by flipping the coil (Figure 3.4). Other stimulus parameters were similar to those in previous experiments (delay of magnetic stimulation, 106 ms; visual pattern, a grid of 1.5 cycles/deg).

Figure 3.4 illustrates the scotomas for the different electric field directions for a representative subject (among four). Consistent with the report by Amassian *et al.* (1994),

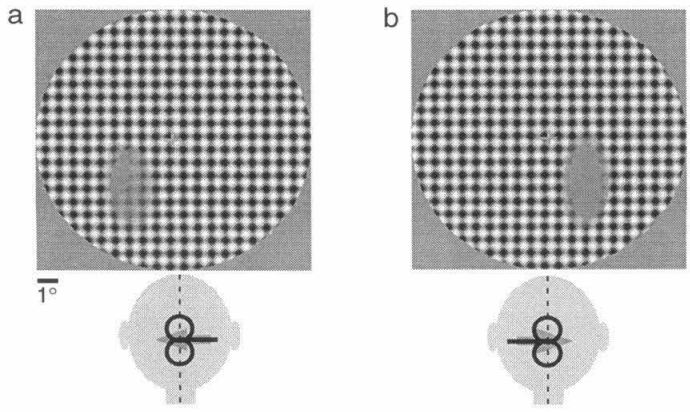

Figure 3.4: Effect of electric field directions
Reconstructed percepts (top) are shown with schematic illustrations of coil configuration and the electric field direction (indicated by an arrow). (a) and (b) are for leftward and rightward electric fields, respectively.

when the electric field is leftward (rightward), the scotoma was seen in the left (right) visual field, presumably because the right (left) hemisphere was effectively stimulated. In all subjects, the location of scotomas showed the same dependency on the electric field direction, though some reported weaker scotomas in the other side of the visual field. The figure shows vertically elongated scotomas, but this feature was not consistent across subjects.

Dependency on the electric field direction is a ubiquitous phenomenon with TMS, which was first reported in the motor cortex (Barker *et al.*, 1987; Rothwell *et al.*, 1993). The orientation of neural fibers as well as the difference in impedance between different brain tissues (gray and white matter, ventricles, etc.) has been suggested as the source of the direction dependency (Amassian *et al.*, 1994), though the biophysical mechanism is not well understood (see Chapter 8).

Chapter 4 Spatial interactions with visual stimuli

4.1 Scotomas and completion

In the previous chapter, we have observed that TMS-induced suppression can be directly visualized as a scotoma in a large-field, flashed visual pattern. The agreement of our findings with physiological and anatomical facts as well as previous TMS studies provides support for the validity and efficiency of our technique in identifying the suppressive effect of TMS. It should be noted, however, that while previous studies had demonstrated that performance on a visual target is degraded by TMS, this did not necessarily imply that a scotoma would be visualized in a large-field pattern.

In cases of cortical blindness and homonymous hemianopia, which occurs due to postchiasmal or cortical lesions (Bergman, 1955; King, 1967), even though the patients have difficulty with the task of identifying visual targets presented in the visual field corresponding to the lesion, many of them do not perceive the visual field deficit as a region lacking patterns or objects in a visual scene. Instead, the deficit region is perceptually completed or "filled-in" with the neighboring visual information.

It is known, however, that patients with cortical lesions, who usually demonstrate the completion in visual scenes, perceive a scotoma in flickering random-dot patterns (Schiefer *et al.*, 1998). Such visual stimuli may be too transient and irregular to be completed. The TMS-induced scotoma also seems to indicate the failure of such completion. In the scotoma display, the visual stimulus may be too brief for the completion to be fully carried out.

Is it possible, however, to observe hints of the completion process in TMS-induced scotomas? In the following sections, we describe spatial distortion effects of TMS-induced scotomas created on various spatial visual patterns, which could be thought of as "incomplete" completion.

4.2 Spatial visual pattern and the shape of scotoma

4.2.1 Distortion in grating patterns

When a horizontal or vertical grating (contrast, 100%; 0.9-1.5 cycles/deg; duration, 40 ms) was flashed followed by a magnetic pulse (delay, 106 ms), we found that the shape of the scotoma depended on the pattern (Figure 4.1). The scotoma was perceived as horizontally compressed when a horizontal grating was presented (Figure 4.1 a) and vertically compressed when a vertical grating was shown (b), relative to the scotoma seen with a grid (superimposed vertical and horizontal gratings of 50% contrast) (c). In one of seven subjects, however, the scotoma tended toward a horizontally compressed shape regardless of the pattern. We calculated the aspect ratio of the ellipses for each subject and pattern (the mean length of the axes orthogonal to the pattern's orientation across five repeated trials divided by that of the parallel ones). It ranged from 1.3 to 3.2 for those who observed the pattern-dependent distortion.

To see if the distortion resulted merely from the short duration of the visual stimulus, we presented gratings containing a circular, gray patch comparable in size to the scotoma for 40 ms without TMS. In this case, little distortion was observed. Therefore, the anisotropy was not simply due to the brief presentation of the visual stimulus.

Relative to the scotoma in the grid pattern, the scotomas in the gratings were generally more compressed along the stripes than elongated in the directions perpendicular to them; that is, the stripes in the gratings seemed to extend into the scotoma. In addition, the scotoma in the grid pattern did not match the superposition of those observed separately with horizontal and vertical gratings, even when the contrast of the horizontal and vertical gratings was reduced to 50% for a better comparison with those composing the grid.

It could be argued that the anisotropic distortion may simply reflect the elliptical shape of the classical receptive fields of cells tuned to the pattern's orientation that are inhibited by the magnetic stimulation. However, the receptive fields of most simple cells are elongated along, rather than perpendicular to, the preferred orientation (Jones & Palmer, 1987). Therefore, TMS would be expected to affect an elongated region parallel to the orientation of the pattern. Furthermore, classical receptive field shape would not explain differences between the scotoma in the grid and the superposition of those seen separately with horizontal or vertical gratings, unless one assumes some nonlinear interactions among

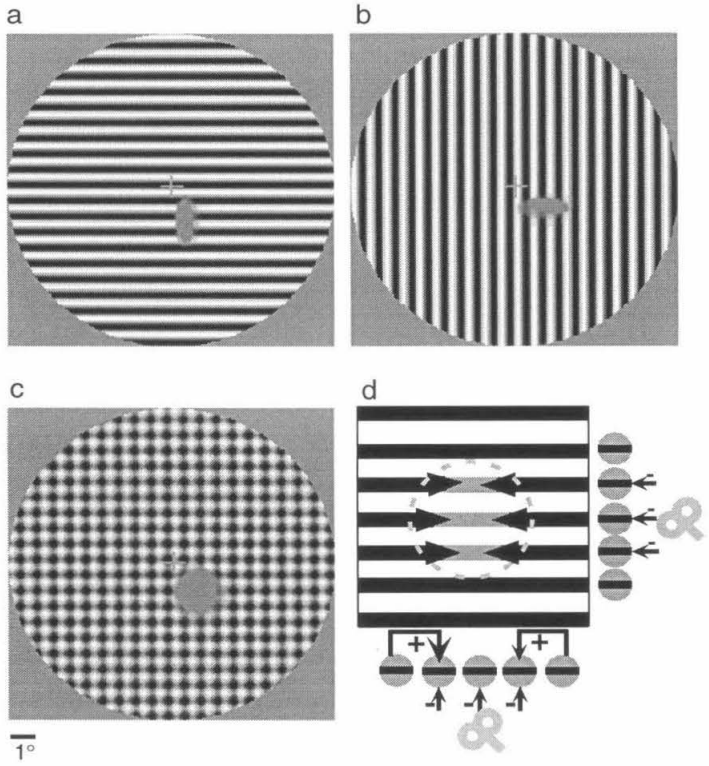

Figure 4.1: Distortion of scotomas on grating patterns
(a-c) Reconstructed percepts of a subject for horizontal (a) and vertical (b) gratings, and a grid pattern (c). (d) Hypothetical mechanism for the anisotropic distortion of the scotoma. A horizontal grating is shown with horizontally tuned neural units aligned vertically (right) and horizontally (bottom). The central gray circle represents the visual space corresponding to the cortical area affected by TMS. Long-range facilitatory connections among collinearly aligned units (+ in the bottom row) mask inhibition by TMS (indicated by −); thus, the scotoma appears compressed along the stripes.

receptive field mechanisms.

A more satisfactory account may be provided in terms of long-range facilitatory connections and nonlinear interactions among classical receptive field mechanisms with a similar preferred orientation and collinear alignment. The mechanisms are suggested by anatomical (Gilbert *et al.*, 1990), electrophysiological (Kapadia *et al.*, 1995; Polat *et al.*, 1998), and psychophysical (Polat & Sagi, 1993) studies, and may be involved in various kinds of completion phenomena. The long-range facilitation by collinear stimuli, most pronounced in cells firing at near-threshold level (Polat *et al.*, 1998), may counter inhibition triggered by magnetic stimulation. As facilitation occurs only along the stripes, it produces the anisotropic shape of the suppressed region (Figure 4.1d). The large, round scotoma observed in the grid pattern may reflect attenuation of the facilitatory effect between collinear lines by the presence of orthogonal ones, as observed in monkey V1 (Kapadia *et al.*, 1995), which would inhibit extension of the perceived stripes. Thus, the distortion of the scotoma may be regarded as a result of "incomplete" completion.

4.2.2 Distortion in radial and concentric patterns

To further confirm the compression of the TMS-induced scotoma along stripes, we compared the suppressed areas within radial, concentric and grid patterns (Figure 4.2). As the spatial frequency of a "true" radial pattern varies with the distance from the center, and visual processing time varies with spatial frequency, the center and the periphery thus seemed to appear asynchronously when the pattern was flashed, confusing the perception. Therefore, radial and concentric patterns were actually composed by rearranging the horizontal and vertical gratings as shown in Figure 4.2a and b. The centers of the radial and concentric patterns were positioned at the center of the scotoma as determined by flashing the grid pattern for each subject. The temporal parameters were identical to those in the previous experiment (stimulus duration, 40 ms; delay of magnetic stimulation, 106 ms). We predicted that the scotoma in the radial pattern would be smaller than those in the other patterns because of the extension of stripes toward the center of the scotoma.

Four subjects showing anisotropic distortion with gratings perceived the area of the scotoma as smallest in the radial pattern (Figure 4.2a) and largest in the grid pattern (c). The ratio of the suppressed area in the radial pattern to that in the grid pattern ranged from 0.51 to 0.85, confirming that the TMS-induced scotoma was compressed along stripes.

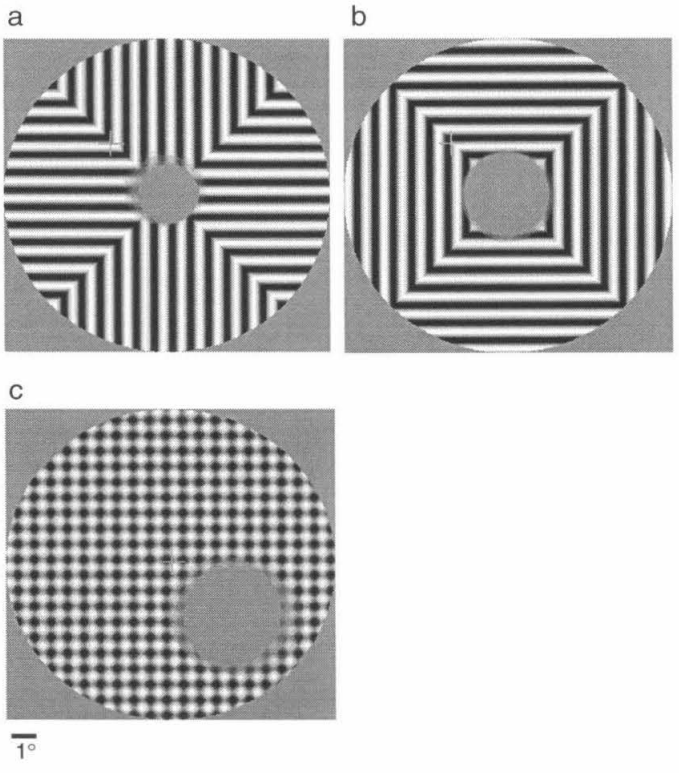

Figure 4.2: Distortion in radial and concentric patterns
Reconstructed percepts of a subject for a radial (a), concentric (b) and grid (c) patterns. The radial and concentric patterns were presented away from the fixation point such that the scotoma was observed in the center of the patterns.

The larger size of the scotoma in the grid pattern may indicate strong inhibition of stripe extension in the presence of the orthogonal stripes.

4.3 Scotomas in illusory contours

Visual patterns are not limited to those defined by luminance, which have been used so far. We are able to perceive visual features which are not explicitly given to the retina. A striking example is illusory contours. Such contours are induced by luminance-defined (real) stimuli, such as abutted lines and fan-shaped stimuli (Kanizsa, 1979), but perceived at locations where the inducing stimuli are not presented. There is increasing evidence showing that early visual cortices, including V1, are involved in the detection of illusory contours, and that illusory and real contours are processed similarly at anatomically overlapping sites (von der Heydt & Peterhans, 1984; Grosof *et al.*, 1993; Sheth *et al.*, 1996; Larsson *et al.*, 1999; Mendola *et al.*, 1999; Seghier *et al.*, 2000). Since TMS of the occipital lobe is thought to interfere with early visual cortices (Kastner *et al.* 1998), it may affect cortical processes involved in the formation of illusory, as well as real, contours. Here, we extend the paradigm of the spatial distortion of scotomas to illusory contours defined by abutted line segments to examine the similarity to real patterns.

4.3.1 Distortion in real and illusory patterns

We replaced the sinusoidal patterns used so far with patterns composed of thin luminance-defined lines (line width, 0.09 deg; line luminance, 46.3 cd/m^2; background luminance, 16.7 cd/m^2). Three kinds of real and illusory patterns were created by arranging the lines as detailed below. The visual patterns were presented for 80 ms followed by a magnetic pulse with a delay of 146 ms. Otherwise, the stimulus parameters were identical to those in the previous experiments.

First, we presented a real grating (2.3 cycles/deg; horizontal or vertical) composed of the thin lines as shown in Figure 4.3a. The TMS-induced scotoma was compressed vigorously along the orientation of the grating in all four subjects, replicating the original effect observed with the sinusoidal gratings. Second, an orthogonal illusory grating (2.3 cycles/deg) was formed by breaking and shifting the lines in the real grating (Figure 4.3b). In this pattern, the compression was substantially attenuated, and the area of the scotoma

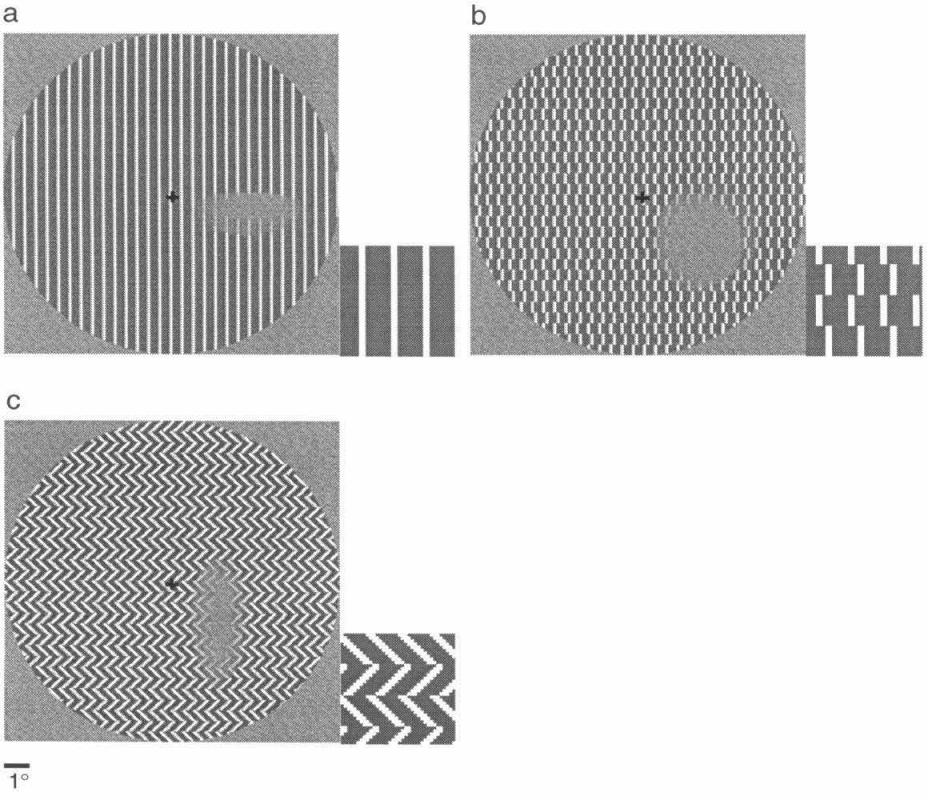

Figure 4.3: Distortion of scotomas in real and illusory patterns
Reconstructed percepts of a subject for real (a) and illusory (b,c) patterns. Magnified patterns are shown on the right. The pattern (b) is created by breaking the lines in (a). In the pattern (c), an illusory grating as in (b) is made of oblique inducers (45 and 135 deg).

became larger. No consistent and substantial anisotropy across subjects was observed. It was possible, in theory, to perceive independent scotomas for the illusory and real (due to the inducers) components of the pattern. However, subjects did not see such multiple regions, but reported a single, roughly elliptic region.

Even though the orientation of the illusory grating was 90 deg different from the original real grating, the direction of distortion was not completely reversed. This may be due to the interaction of two potential compression effects, one along the real line segments and the other along the illusory contours. They may inhibit each other producing a less compressed, larger scotoma.

To isolate and reveal the potential component of the compression induced by illusory contours, an illusory grating with oblique inducers was employed (Figure 4.3c): the line segments of every other column (row) in the previous pattern were oriented 45 deg or 135 deg. Since there were two orthogonal sets of oblique inducers, the compressive effects from the real lines were expected to be canceled, and the effect of the illusory contours should become dominant. Indeed, a substantial compression along the illusory contours was observed in all subjects. Thus, distortion in illusory gratings was found to be qualitatively similar to that in real gratings.

4.3.2 Stimulus duration and distortion

It is known that, compared to real patterns, a longer duration is necessary for illusory contours to be perceptually effective (Ringach & Shapley, 1996; Gegenfurtner *et al.* 1997). Here, we show data obtained when the illusory grating composed of orthogonal lines (Figure 4.3b) was presented for 53 and 107 ms as well as 80 ms to alter the perceptual vividness of the illusory contours. We wondered whether the distortion along illusory contours would be modulated accordingly.

Figure 4.4 shows the horizontal to vertical ratio of the matched ellipses (the mean of the horizontal axes divided by that of the vertical ones) for a subject as a function of the duration of presentation. Even though the pattern did not lead to consistent and significant distortion across subjects (three) with 53 and 80 ms durations, it produced significant compression along the orientation of the illusory contours when presented for 107 ms. Thus, the distortion was sensitive to the duration of the visual pattern. In our pilot study, however, the delay of TMS from the onset of the visual stimulus did not strongly

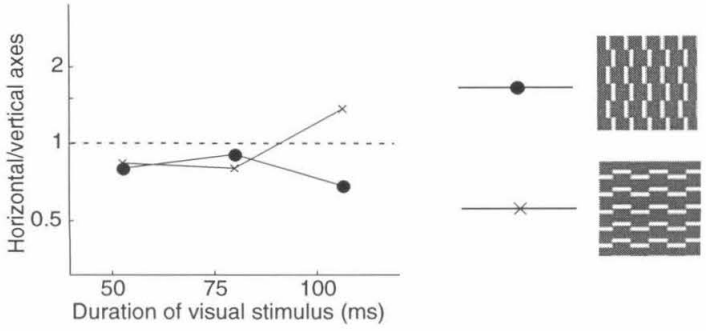

Figure 4.4: Duration of illusory contours and distortion
The horizontal to vertical ratio of the scotoma is plotted in logarithmic scale for a subject. The filled circles and x's indicate the data for horizontal and vertical illusory gratings (induced by vertical and horizontal lines), respectively.

affect the degree of distortion, within the range where a clear scotoma was perceived.

The distortion of scotomas according to the orientation of illusory contours indicates that they are processed in early visual cortices, which can be affected by TMS of the occipital lobe. It is difficult, however, to resolve whether the stimulation occurs at V1 or V2/3 (or both) because of spatial limitations of the current TMS technique (Kastner *et al.*, 1998). The similar compression effects suggest common mechanisms underlying the perception of illusory and real contours/lines, though illusory contours seem to require more time to form established cortical representation. TMS of the occipital lobe may interfere with progressive stages of visual processes, which are involved in the perception of contours/lines, irrespective of whether they are illusory or real.

4.4 Distortion of afterimages

Is the distortion in a grating pattern a phenomenon peculiar to TMS-induced scotomas? If it indicates some general cortical processes, such as the long range facilitation which may be involved in various perceptual completion phenomena, similar distortion may be observed in other situations. We found that afterimages show similar, though weak, distortion when perceived on a grating pattern.

An afterimage was created by viewing a small white disk (46.7 cd/m^2; diameter, 1.8

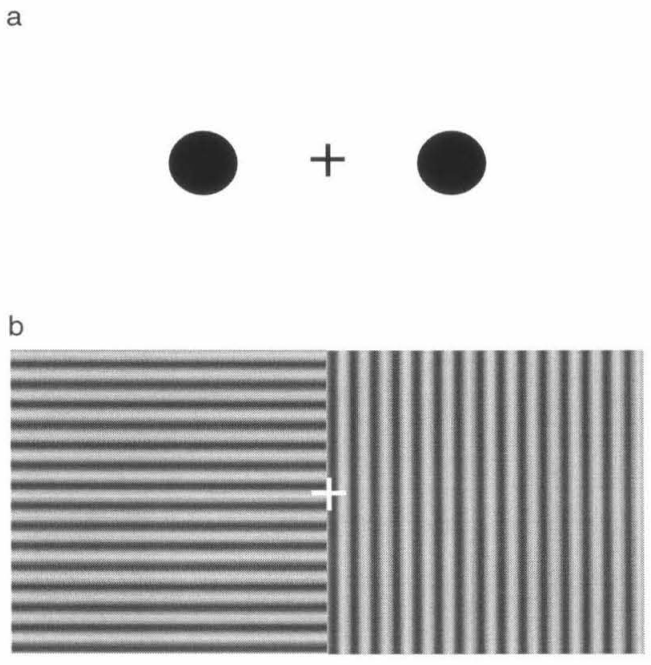

Figure 4.5: Distortion of afterimages
Fixate to the cross in (a) for about 20 sec, creating the afterimages of the two disks. Then, move to the cross in (b), projecting the afterimages on the gratings. Compare the shapes of the afterimages on the left and the right. The effect may be more vividly reproduced on a CRT monitor displaying similar images.

deg; position, 1.1 deg right of and below the center) on a dark background (0.1 cd/m^2), or a disk and background with the reversed luminance, for 20 sec with the eyes fixated to a central fixation point. Then, the visual stimulus was replaced with a vertical or horizontal sinusoidal grating (contrast, 50%; mean luminance, 22.3 cd/m^2; 3.4 cycles/deg).

The afterimage typically built up for the first few seconds, and faded away (then, weakly faded in and out again). Its shape appeared to be distorted depending on the background pattern: on a horizontal grating, the afterimage was horizontally compressed (vertically elongated), and on a vertical grating, it was vertically compressed (horizontally elongated). Figure 4.5 demonstrates this basic phenomenon, where one can compare the shapes of the afterimages on the horizontal and vertical gratings simultaneously.

4.4.1 Comparison with luminance-modulated images

We measured this distortion by having the subject draw an ellipse to match the afterimage. After viewing the afterimage projected on the grating at least for 3 sec, the subject indicated the size, shape and location of the afterimage based on its clearest percept, by drawing an ellipse as in the previous experiments measuring the scotoma.

To see if the distortion was simply due to the brightness configuration created by the afterimage projected on the grating, we also measured the distortion in real visual stimuli where the luminance of the disk region in the grating was decremented (corresponding to the afterimage by the positive disk) or incremented (the negative disk) by 5.6 cd/m^2. To make the real images comparable to the afterimage, the edge of the disk region was blurred by convolution with a Gaussian function ($\sigma = 0.13$ deg), and the luminance was modulated only for 2 sec. The luminance and the degree of blurring were based on the preliminary observation of afterimages projected on a gray homogeneous background. After the luminance modulation ended, the observer reproduced the shape, size, and location of the disk region in the same way as in afterimage trials.

Figure 4.6 shows the ratio of the orthogonal to parallel axes (relative to the orientation of the background grating) of the ellipses for all four subjects. The results for horizontal and vertical backgrounds are pooled in each subject since they are similar. The ratio of orthogonal to parallel was calculated by dividing the mean length of the orthogonal axes divided by that of the parallel ones for each subject. Results are shown only for the afterimages by the white adapting disk and for the corresponding real images with luminance decrement. The results were similar for the conditions of the opposite polarity. In all subjects, the orthogonal to parallel ratio of afterimages was largely above one, indicating the compression along (elongation orthogonal to) the orientation of the grating (Figure 4.6a), whereas that of real images was close to one, though generally slightly above one (b).

We also analyzed the absolute size of the distorted afterimages to see whether the distortion is due to compression in the axis parallel to the grating, or due elongation in the orthogonal axis (or both). The axis lengths were compared with those of the afterimages perceived on a gray homogeneous background. In all subjects, there was significant compression along the parallel axis (t-test, $p < .05$), while two of them showed significant elongation in the orthogonal axis ($p < .05$), too.

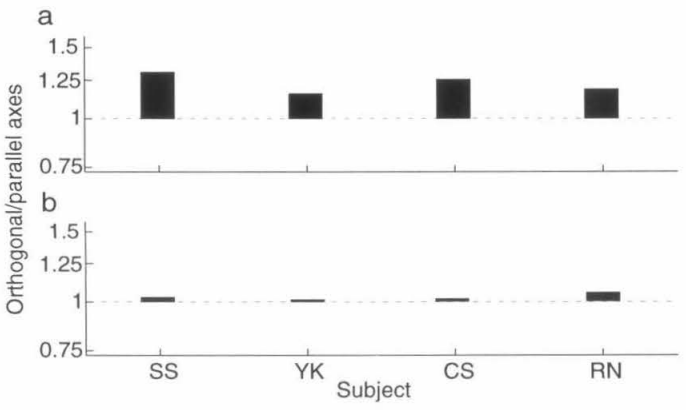

Figure 4.6: Distortion of afterimages and real images
The ratios of the orthogonal to parallel axes (relative to the orientation of the background grating) are plotted in logarithmic scale for afterimages (a) and luminance-modulated images (b). The results for horizontal and vertical backgrounds are pooled.

We have seen that only weak distortion, if any, was observed in real images simulating the brightness modulation by afterimages. This rather quantitative difference, however, might be simply due to the failure to precisely replicate the brightness modulation by afterimages. To demonstrate qualitative difference between afterimages and real images, we explored the following phenomenon.

We noticed that strong distortion could be observed in real images when the background grating had a low spatial frequency relative to the disk size (Figure 4.7a and b). The direction of distortion, however, could be either the same as or opposite from that of afterimages in the previous experiment, depending on the polarity, or phase, of the background grating. The disk region in Figure 4.7a appears horizontally compressed, while in Figure 4.7b, where the polarity of the grating is reversed, it appears rather horizontally elongated. Similar drastic shape changes occurred as long as the disk was centered at a positive/negative peak of a low frequency grating, and the edge was blurred. This seems to be due to the fact that the perceived edge location of the blurred disk is dependent on the background luminance: in Figure 4.7a and b, for example, the edge on the dark phase of the grating is localized outer than the edge on the bright phase. It may affect the overall shape perception especially when the disk overlaps with only a few cycles of the grating.

Do afterimages show the same polarity dependency with a low spatial frequency grating?

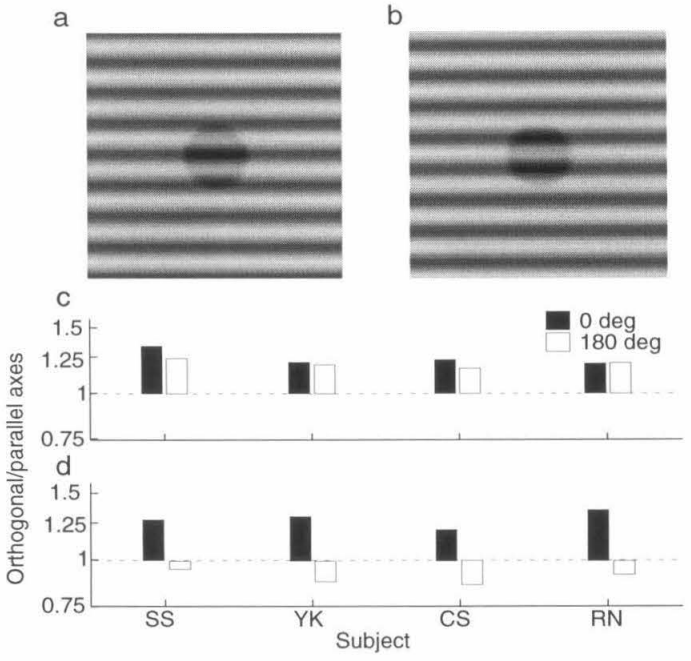

Figure 4.7: Effect of polarity in low-frequency gratings
(a, b) The intensity in a disk region of a grating is decremented. The polarity of the background grating is reversed in (a) and (b), yielding opposite directions of distortion. The reversal of the polarity of the disk, instead of the grating, had the same effect. (c, d) The orthogonal to parallel ratios of afterimages (c) and real images (d) are plotted for each subject and background polarity ("0 deg" or "180 deg"). "0 deg" and "180 deg" refer to the configurations of the disk and the grating similar to (a) and (b), respectively.

The distortion of afterimages and real images were measured in the same manner as in the previous experiment, using low spatial frequency gratings (1.1 cycles/deg) of different polarities. We refer to the polarities (or relative phases between the disk and the grating) producing the distortions as in Figure 4.7a and b as "0 deg" and "180 deg," respectively. In this experiment, only the white adapting disk and the corresponding decremented images were used. Since the relative phase between the afterimage and the background grating can vary with eye movements, in selected trials, the subject's eye movements were monitored with an infrared eye tracker. Also, subjects monitored their own eye movements through the movements of the afterimage. We rejected the trials where subjects reported failure to fixate.

As shown in Figure 4.7c and d, both afterimages and real images were strongly distorted. However, the pattern of distortion was totally different: afterimages were compressed along (elongated orthogonal to) the orientation of the grating, regardless of the background polarity (Figure 4.7c), while in real images, different polarities led to the opposite directions of distortion (d), confirming the phenomenology described above. These results demonstrate a qualitative difference in distortion pattern between afterimages and real images.

The failure to reproduce the distortion of afterimages with luminance-modulated visual stimuli indicates that the process by which the brightness is modulated, rather than the outcome of the modulation, is critical for the distortion. Therefore, the state of adaptation, by which neural signals and the corresponding brightness are modified, may be affected by the cortical orientation-dependent activity to produce the distortion.

4.4.2 Comparison with TMS-induced scotomas

We have shown that TMS-induced scotomas and afterimages show qualitatively similar distortion. Mere similarity at the phenomenological level, however, does not immediately indicate a common underlying mechanism. To assess the similarity at the level of mechanisms, dependency of the distortion on various stimulus parameters should be investigated. Here we compare TMS-induced scotomas and afterimages using background gratings of various spatial frequencies. To make the spatial parameters comparable, the size and location of the adapting disk for afterimages were determined based on those of the scotoma for each subject.

First, TMS-induced scotomas were recorded with the ellipse drawing procedure using

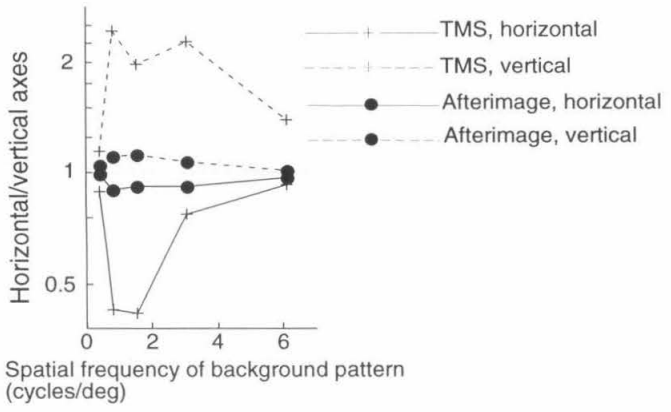

Figure 4.8: Comparison of TMS-induced scotomas and afterimages
The ratios of the horizontal to vertical axes are plotted as functions of the spatial frequency of the background for a subject. The crosses and filled circles indicate the TMS and afterimage conditions, respectively. The solid and broken lines show the data for the horizontal and vertical backgrounds, respectively.

background gratings of various spatial frequencies (1.7, 3.4, 6.7, 13.4, and 26.8 cycles/deg). The grating was presented for 40 ms, followed by a magnetic pulse with a delay of 106 ms. Second, the afterimage experiment was conducted using an adapting disk with a position and diameter which are identical to the mean position and the mean length of the longer axes of the TMS-induced scotomas, respectively. The afterimages were projected on the backgrounds of the same spatial frequencies, and were recorded with the same method as in the previous experiments.

Figure 4.8 shows the ratios of the horizontal to vertical axes of the ellipses (H/Vs; the mean horizontal length divided by the mean vertical length) of TMS-induced scotomas and afterimages as functions of the background frequency for a representative subject (among three). The distance from the dotted line (H/V = 1) represents the degree of distortion. Overall, the degree of distortion was much smaller in afterimages than in scotomas. The peaks of H/V for scotomas on horizontal (vertical) gratings ranged 0.40-0.41 (2.2-2.6) across subjects while those for afterimages ranged 0.85-0.90 (1.1-1.3). Scotomas and afterimages, however, showed a similar overall profile: little distortion was observed at very low and high spatial frequencies, and the degree of distortion peaked at intermediate frequencies (1-3 cycles/deg). The curves peak at slightly lower spatial frequencies compared to the

contrast sensitivity functions at given eccentricities (Rovamo & Virsu, 1979), though they fall within the range of the spatial frequency tuning of striate cortical cells of the monkey (DeValois *et al.*, 1982).

The results demonstrate that despite the difference in the degree of distortion, the shapes of TMS-induced scotomas and afterimages are similarly affected by the background spatial frequency. Such similarity further supports the idea that the distortion effects in TMS-induced scotomas and afterimages share common underlying mechanisms.

As in adaptation, it is known that TMS can change neural excitability or responsiveness in addition to producing or inhibiting neural signals (Valls-Solé *et al.*, 1992; Hallet, 1995; Pascual-Leone *et al.*, 1999). Therefore, we speculate that orientation-dependent neural activity may effectively interact with mechanisms controlling neural excitability involved in TMS and adaptation.

Since retinal adaptation (Craik, 1940; Brindley, 1959; Wilson, 1997) is unlikely to directly interact with orientation-dependent mechanisms, which mostly exist in the cortex, the distortion effect may suggest the involvement of cortical adaptation (Movshon & Lennie, 1979; Maffei *et al.*, 1973; Ohzawa *et al.*, 1985) in the formation of afterimages. On the other hand, since TMS of the occipital cortex affects mostly the cortex, TMS-induced scotomas may be more directly malleable to cortical orientation-dependent processes than afterimages, which may have both retinal and cortical origins. Thus, the degree of cortical involvement in the origins of TMS-induced scotomas and afterimages may account for both the similarity and the difference in their distortion.

Chapter 5 Temporal interactions with visual stimuli

5.1 Temporal filling-in to scotomas

A fundamental question as to a perceptual quality of the TMS-induced scotoma has remained unanswered: why is the scotoma visualized as gray? Gray may be a result of reduced spatial contrast of the flashed pattern, or a "default value" in perception corresponding to suppressed neural activity. It should be noted, however, that the visual pattern was presented on a gray background, thus the pattern was temporally sandwiched between gray fields. Hence, it may also be possible that the gray in the scotoma resulted from filling-in with the visual features temporally adjacent to the flashed stimulus.

To address this issue, we presented colored rather than gray homogeneous fields (18.0 cd/m^2) for more than 1 sec both before and after a flashed grating (mean luminance, 22.3 cd/m^2; contrast, 100%) (Figure 5.1). Since the flashed pattern was perceived less clearly when presented between colored fields, the grating was presented longer (80 ms) than in previous experiments. The delay of the magnetic stimulation was set to 106 or 120 ms. After drawing the scotoma, the subject selected the perceived color of the scotoma: the color of the ellipse changed with the horizontal position of the mouse, corresponding to the degree of the mixture of gray and the colors presented before and after the grating. When the grating was presented between red fields and followed by a magnetic pulse, all subjects (five) reported that the scotoma appeared close to red (Figure 5.1a), suggesting that the scotoma was filled in with temporally adjacent stimuli.

Next, to see whether the filled-in information was from the preceding or subsequent backgrounds, homogeneous fields of red or green were presented before and after the grating (Figure 5.1b and c). Subjects consistently reported the color of the scotoma to be closer to that presented after the grating, though apparent color saturation varied across subjects. No one reported yellowish color, a mixture of red and green. Results were similar over the range of delays that produced clear, localized suppression.

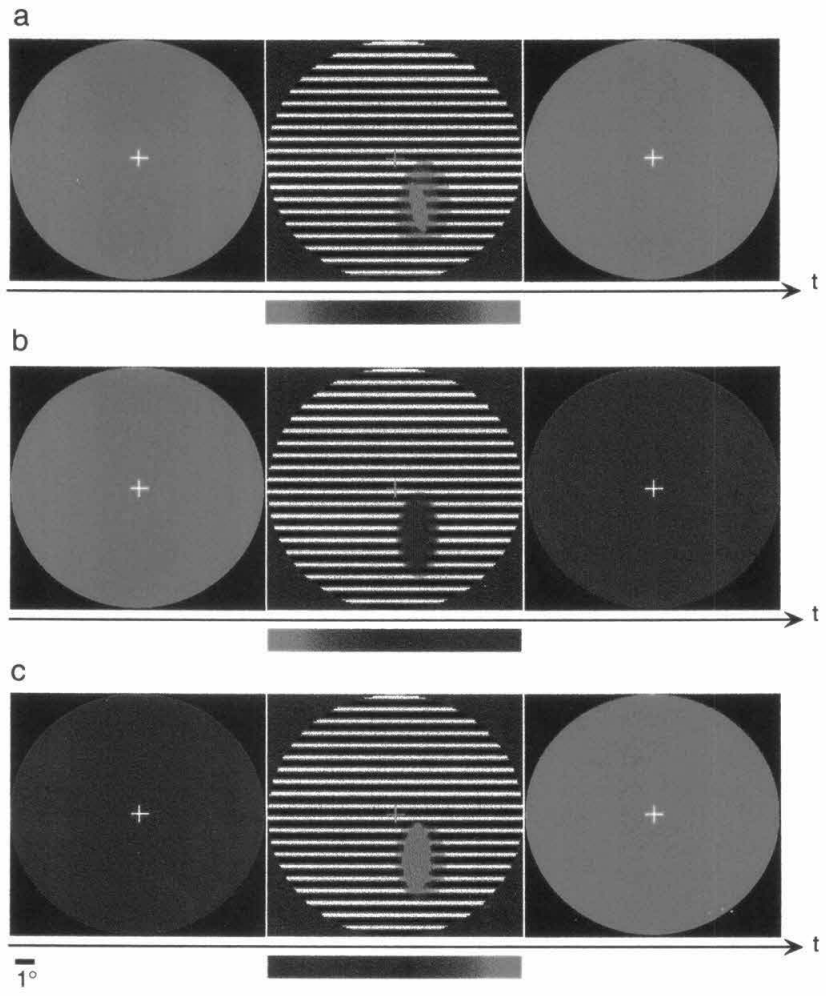

Figure 5.1: Temporal filling-in to scotomas
Reconstructed percepts of a subject in a flashed grating (middle) and colored fields presented before (left) and after (right) the grating. The perceived color of the scotoma was selected from a gradient scale of gray and red/green as shown below the middle panels. The color for each pixel was averaged over five repeated trials. Note that, as the presented grating was horizontal, the suppressed regions were horizontally compressed.

As is observed in backward masking (Weisstein, 1971; Breitmeyer, 1984), this phenomenon indicates that the subsequent stimulus (the following color) affected perception of the previous stimulus (the flashed grating). Thus, we term it "backward filling-in." This seemingly puzzling phenomenon might be reasonably explained by assuming that, without TMS, the grating masks and thus delays perception of the following colored stimulus; magnetic suppression of this forward masker may lead to local disinhibition, and thus earlier visibility, of the following color. Given this account, this phenomenon seems analogous to the finding that TMS can block backward masking of a visual target by suppressing the masking stimulus (Amassian *et al.*, 1993). However, note that in this kind of "unmasking," a backward masker is suppressed by TMS, whereas we assume suppression of a forward masker. Furthermore, unmasking does not necessarily imply temporal filling-in of the suppressed region.

The temporal filling-in to scotomas demonstrates that the effect of TMS on visual perception is not simply to interrupt a visual scene momentarily; instead, it is perceived as a result of interactions with the visual stimuli. In this regard, the temporal filling-in is analogous to the distortion effect of the scotoma, which was a product of the spatial interaction with the visual pattern. Furthermore, the temporal filling-in, like the spatial distortion, suggests a process that serves for the completion of weak or absent information.

5.2 Suppression of transient changes

As discussed in the previous section, percepts in the scotoma region seem to reflect intriguing temporal interactions between visual and magnetic inputs. The scotoma display, however, may be too complicated to specifically observe the temporal characteristics of TMS-induced suppression. In this section, we investigate them using simple and small visual targets that fall within the scotoma region. In particular, effects of TMS on transient aspects of visual stimuli are explored, since they seem to be effectively suppressed by TMS as suggested by the observation that the scotoma was created only in a flashed visual stimulus, but not in a steadily shown stimulus (Chapter 3).

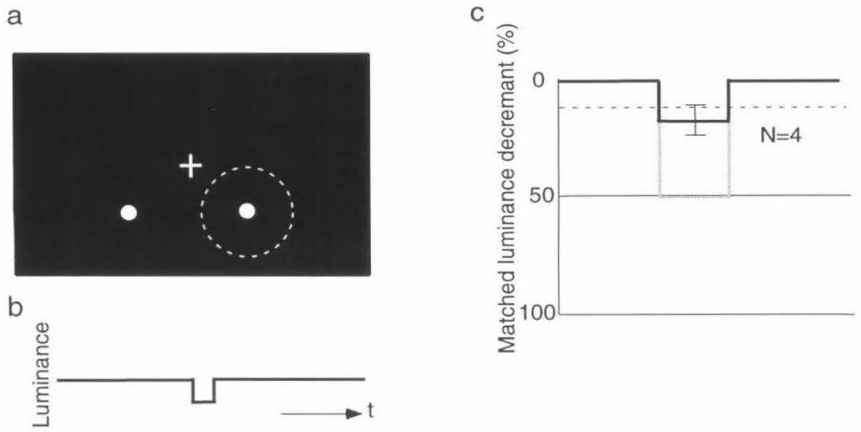

Figure 5.2: Suppression of brief luminance decrement
(a) Spatial configuration. Two small disks were presented at horizontally symmetrical locations with respect to the central fixation point (cross). One of the disks was inside the scotoma region (dotted circle). The other was used to measure the perceived decrement of the disk in the suppressed region (b) Temporal profile. The luminance of the disk inside the scotoma was decremented for 27 ms by 50%, while that of the other disk was decremented simultaneously by a value adjusted by the subject. (c) The mean of the matched luminance decrement for four subjects is plotted relative to the full decrement to the background luminance (solid line). The error bar represents standard deviation. The gray line indicates the actual decrement of the disk in the scotoma region. The dotted line shows the mean threshold of detectable decrement.

5.2.1 Brief luminance decrement

First, we studied the effect of TMS on a brief luminance decrement of a visual target located within the suppressed region. Unlike a "flashed" stimulus, the magnetic suppression of it could result in opposite effects depending on whether TMS reduces brightness (or perceived spatial contrast), or its temporal change (Figure 5.2). If brightness or spatial contrast is suppressed by TMS, the perceived decrement would be enhanced, while if the temporal change is suppressed, the impression of the decrement would be attenuated.

A small white disk (46.7 cd/m^2; diameter, 0.4 deg) was presented on a black background (0.1 cd/m^2), such that it was located within the suppressed region (dotted circle in Figure 5.2a) measured with the scotoma procedure using a grid pattern and TMS of the left occipital lobe (coil center, 2-3 cm left of and above the inion). The disk center was typically 2.5 deg right of and below the fixation point. The luminance of the disk was decremented

by 50% for 27 ms (Figure 5.2b), followed by a magnetic pulse with a 80 ms delay from the beginning of the decrement. The parameters for magnetic stimulation were set to be effective for suppression of a flashed visual stimulus. Another disk of the same luminance and size was shown at the horizontally symmetrical location, i.e., outside the suppressed region. Its luminance was also briefly decremented by a variable value simultaneously with the disk inside the suppressed region. The subject adjusted the luminance decrement of the disk outside the suppressed region using a computer mouse, repeating the observation until the perceived luminance decrement of the two disks appeared equal. Each subject performed three trials of adjustment (each trial consisted of five to six observations on average). In a separate session, the threshold for the visibility of the luminance decrement was measured by adjusting the luminance level without magnetic stimulation.

Figure 5.2c shows the matched luminance decrement for four subjects. The perceived decrement in the scotoma region is attenuated compared to the actual decrement (50%). Furthermore, the matched decrement was close to the threshold of detectable decrement (dotted line). Subjects reported that in many trials, they did not notice any change in the disk of the scotoma region. Some of them also experienced perceptual delays of the decrement in the suppressed region. The results support the idea that transient changes, rather than brightness or spatial contrast, are effectively suppressed by TMS. This is also consistent with the finding that the percept in the scotoma is not simply a result of reduced spatial contrast of the flashed pattern as shown in the temporal filling-in phenomenon.

5.2.2 Timing of appearance and disappearance

Briefly flashed visual targets, which have been commonly used with TMS, consist of two temporal phases: appearance and disappearance. We next studied the effect of TMS on the perceived timing of each of them, using an abruptly presented or extinguished (otherwise, steadily shown) stimulus in a similar configuration as in the previous experiment.

A disk located within the suppressed region (dotted circle in Figure 5.3a) was abruptly turned on or off 1.5 sec after the beginning of each trial, and stayed on or off for 1.5 sec (Figure 5.3b). The appearance or disappearance was followed by a magnetic pulse with a delay of 80 ms. Another disk was located at the horizontally symmetrical position (outside the suppressed region). When the two disks were turned on or off physically at the same timing followed by TMS, we found asynchrony in the perceived timing of these events

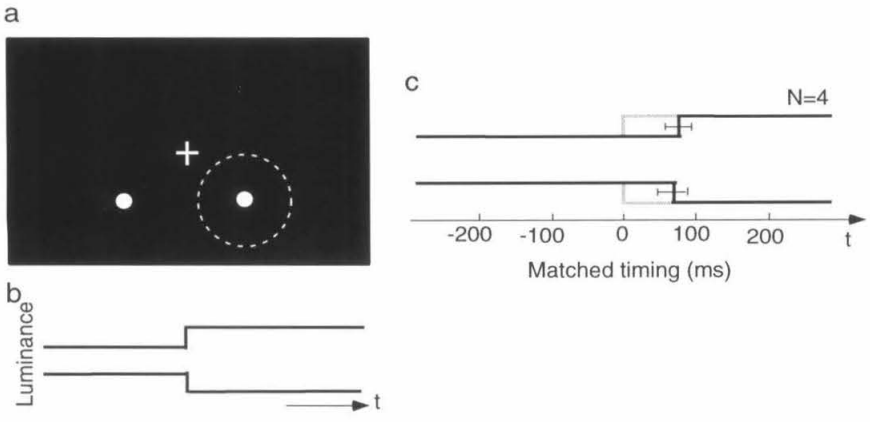

Figure 5.3: Suppression of appearance and disappearance
(a) Spatial configuration. Two small disks were presented at horizontally symmetrical locations with respect to the central fixation point (cross). One of them was inside the region suppressed by TMS (dotted circle). The other was used to measure the perceived timing of the disk in the suppressed region. (b) Temporal profile. Inside the scotoma region, the disk abruptly appeared (top) or disappeared (bottom). The timing for the disk on the other side was adjusted by the subject. (c) Matched timing of appearance (top) and disappearance (bottom). The mean of the matched timing for four subjects (solid line) is plotted relative to the actual timing of the disk in the suppressed region (gray line). The error bar represents standard deviation. Positive values indicate that perceived timing is delayed by TMS.

between them.

To measure the change in the perceived timing caused by TMS, we performed an experiment where the subject adjusted the timing of appearance or disappearance in the disk outside the suppressed region, until the two disks appeared or disappeared perceptually simultaneously. Each subject performed three trials of adjustment for each appearance and disappearance. The spatial configuration and the parameters for magnetic stimulation were the same as those in the previous experiment.

Figure 5.3c shows the matched timing of appearance and disappearance for four subjects. Assuming that a magnetic pulse suppresses the brightness or spatial contrast of the visual stimulus for a certain time period, the initial portion of the appearing disk and the last portion of the disappearing disk are expected to become invisible or attenuated, leading to delayed appearance and early disappearance. However, the results show that the perceived

timing (solid line) for both appearance and disappearance was delayed compared to the actual timing (gray line). In particular, the perceptual delay observed with disappearance is against the prediction based on the suppression of brightness or spatial contrast. It rather seems to suggest that transient changes were suppressed by TMS, resulting in the delay of detection of them regardless of the direction of luminance change.

5.2.3 Color change with a temporal gap

The results of the suppression of a brief luminance decrement (Section 5.2.1), and the delay of appearance and disappearance (Section 5.2.2) are consistent in showing that transient changes, as opposed to brightness or spatial contrast, are effectively suppressed by TMS. The delay of appearance and disappearance, however, seems to be in conflict with the backward filling-in observed in the scotoma (Section 5.1), since the former is a "forward" effect in time. To resolve this apparent inconsistency, the difference in their exact time course should be considered; the display of appearance or disappearance contains only one transient change, while the scotoma display has two transient changes: the appearance and disappearance of the visual pattern. We employed a display where these two cases can be directly compared by changing a single temporal parameter.

Two disks of the same color (red or green; 18.0 cd/m^2) were presented at horizontally symmetrical positions (Figure 5.4a) on the dark background. One of them was shown within the suppressed region as in previous experiments. The disks changed their color simultaneously (red to green, or green to red) with a variable temporal gap (0-160 ms; 40 ms step) (Figure 5.4b). Each color was presented for 1.5 sec. During the gap, only the background and the fixation point was shown. The display of color change with a 0 ms gap is analogous to that of the appearance or disappearance in that they contain only one change in color or luminance. The display of color change with a long gap is similar to that for the backward filling-in, since the gap corresponds to the duration of the flashed visual pattern. A magnetic pulse was applied with a delay of 80 ms from the disappearance of the first color. Thus, the magnetic stimulation was always effective for the disappearance of the first color (the first change), while its effect on the appearance of the second color (the second change) depended on the length of the gap. The subject judged in which disk the second color appeared earlier (two alternative forced choice). The gap duration and the order of the colors were randomized. For each gap duration, 20 trials were repeated.

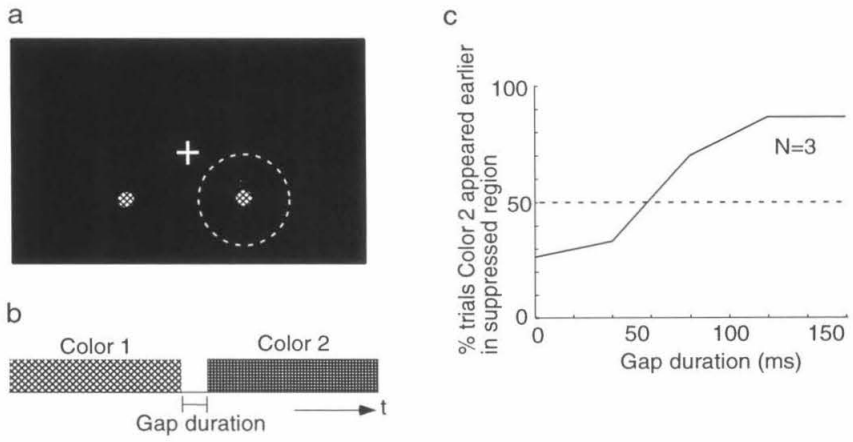

Figure 5.4: Color change with a temporal gap
(a) Spatial configuration. Two small colored disks (red or green) were presented at horizontally symmetrical locations with respect to the central fixation point (cross). One of them was inside the region suppressed by TMS (dotted circle). The other was used for comparison. (b) Temporal profile. Both of the disks simultaneously changed their color from red to green, or from green to red, with a variable gap (0-160 ms). During the gap, only the background and the fixation point was shown. (c) The percentage of the trials where Color 2 appeared earlier in the suppressed region is plotted as a function of the gap duration.

Figure 5.4c shows the percentage of the trials where the second color appeared earlier in the suppressed region as a function of the gap duration (three subjects). When the gap is short or zero, subjects tended to see the appearance of the second color later in the suppressed region, indicating the perceptual delay of change as observed in the appearance/disappearance display. For longer gaps, on the other hand, the second color tended to appear earlier in the suppressed region, consistent with the backward filling-in.

With a short gap, both of the two transient changes may be suppressed by a magnetic pulse, while only the first change may be selectively inhibited when the gap is long. The early appearance of the second color with a long gap may be explained, as the backward filling-in was, by disinhibition of the onset of the second color by the magnetic suppression of the disappearance of the first color, or the onset of the gap. Thus, the display of color change with a variable gap is able to produce results analogous to both the delay of appearance and disappearance, and the backward filling-in. This finding also suggests that the direction of the filling-in to the scotoma may not always be backward, especially when the duration of the visual pattern is short. Additional studies will be required to determine the dependency of the temporal filling-in on parameters of the visual stimuli.

5.2.4 Phase shift in a Gabor patch

In previous sections, we have shown that when a visual target changes its luminance or color only once, the timing of the change can be perceptually delayed by TMS. However, the change itself was still clearly visible in these cases. Is it possible to suppress a change in a visual feature, such that observers do not notice any change in the visual scene? Here we describe a preliminary observation where observers are rather completely blinded to a visual change by TMS, and speculate on the neural basis for the suppression of transient aspects of visual perception.

A Gabor patch (a sine grating whose amplitude is modulated by a 2D Gaussian function) was present in the suppressed region, and the phase of the grating was shifted by 90 deg (Figure 5.5). The phase shift occurred only once, and each of the gratings with different phases was presented for 1.5 sec. This display creates vivid motion perception under normal viewing conditions. When the shift was followed by a magnetic pulse (80 ms delay), however, the patch appeared to be stationary without any change.

This observation is consistent with the finding that TMS can degrade the performance of

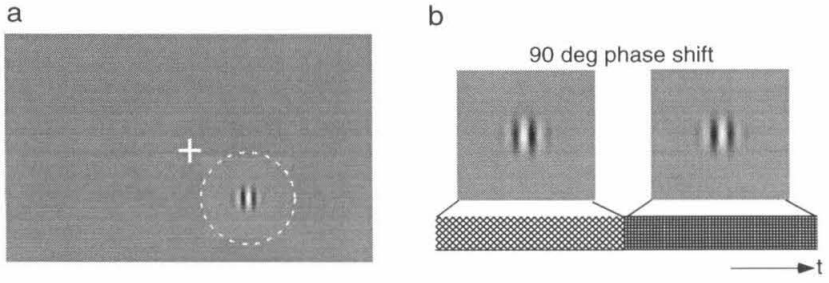

Figure 5.5: Change blindness in motion display
(a) Spatial configuration. A Gabor patch was presented inside the suppressed region (dotted circle). (b) Temporal profile. The carrier (the sine wave component) of the Gabor was abruptly shifted 90 deg, while the envelope (the Gaussian window) remained stationary.

motion direction discrimination (Beckers & Hömberg, 1992; Hotson *et al.*, 1994). In the light of suppression of transient changes, however, the phenomenology of "being stationary," as opposed to the degraded performance in motion discrimination, should be more emphasized.

It is known that we miss remarkable changes in a complex scene with multiple objects when they occur during saccades, eye blinks, or flickering, while under normal viewing conditions, they are easily detectable (change blindness; Rensink, 2000; Pashler, 1988). These studies suggest that our detection of changes in a complex scene largely relies on the signals triggered by the changes, rather than the comparison of the sustained visual features before and after the changes.

As shown in previous sections, the change in luminance or color was delayed by TMS, but did not become invisible. This is presumably because even though the change signals were suppressed by TMS, the display was so simple that the comparison between the sustained features was available to detect the change, though slowly. In the display of a shifted Gabor patch, however, the sustained features were not easily distinguishable due the periodicity and the blurred edge, thus the change was unnoticed when TMS suppressed the change signals.

We have seen that transient aspects of visual stimuli can be prominently affected by TMS. It may be possible that the neural activities induced by sustained and transient stimuli are both similarly disrupted by TMS at early stages, but the effect on sustained stimuli is perceptually obscured due to the completion with temporally and/or spatially adjacent

visual features identical to the disrupted ones. However, neural responses to transient visual stimuli may be rather selectively affected by TMS. The majority of visual cortical neurons are known to respond more vigorously to transient aspects (appearance, disappearance, or drift) of visual stimuli than to sustained aspects (e.g., Schmolesky *et al.*, 1998). Furthermore, in the motor cortex, the effect of TMS is largely enhanced when it is applied during muscle contraction or motor imagery (Rothwell *et al.*, 1991; Kasai *et al.*, 1997), suggesting that active neural states are more susceptible to magnetic stimulation (see also Part II). Therefore, the suppression of transient aspects of visual perception may reflect effective disruption of the active neural responses to visual transients.

5.3 Brightness modulation by paired-pulse TMS

It has been reported that two magnetic pulses with a brief interval (paired-pulse TMS) can reliably produce phosphenes (Boroojerdi *et al.*, 2000). We were recently equipped with a system for paired-pulse TMS. We confirmed that all the observers we tested experienced phosphenes without any accompanying visual stimulus, whereas most of them did not see them with a single magnetic pulse.

Phosphenes are usually tested using a dark, steadily shown background, and they are perceived as transiently brightened, whitish regions. However, this does not necessarily imply that the effect of paired-pulse TMS is simply to add brightness to the background. Alternatively, paired-pulse TMS, like single-pulse TMS, may show nonlinear interactions with the background stimulus. Here, we compare the brightness modulation by paired-pulse TMS in steadily shown and flashed backgrounds of different luminance values.

Two magnetic pulses of the same power were applied to the left occipital lobe with an interval of about 40 ms. The coil position, power, and inter-pulse interval were optimized for phosphene induction on a dark background. Phosphenes were perceived within the lower quadrant of the visual field contralateral to the coil location, similar to scotomas induced by a single magnetic pulse. A large homogeneous disk (diameter, 15 deg) was presented on a dark background (< 0.1 cd/m^2). The disk, at least partly, covered the phosphene region. The disk was set either dimmer or brighter than phosphenes perceived on a dark background. The color of the disk was white/gray, or made close to that of phosphenes if it was substantially different from white/gray. In one condition, the disk was shown steadily

for 6 sec, during which (at the 4th sec) TMS was triggered. In the other condition, the disk was flashed for 95 ms and followed by the magnetic pulses (the first pulse 135 ms after the onset of the flash). The timing was adjusted such that the percept of the disk was modulated by TMS. In order to make the brightness of the flashed and steadily shown disks comparable, we used a longer duration for the flashed disk than in our previous experiments, as a flashed disk of a shorter duration appears darker than the steadily shown one with the same luminance, due to the short temporal summation (Ikeda, 1986). The duration of the flashed disk in this study was long enough to perceive similar brightness as in the steadily shown disk with the same luminance. The subject was instructed to observe the brightness modulation in the phosphene region. After each trial, the disk was redisplayed, and the subject adjusted the luminance of the lower right quadrant of the disk, within which a phosphene had been seen, to match with the brightness modulation. The four conditions (steady/flashed x dimmer/brighter) were randomly repeated five times each.

Figure 5.6 shows the matched luminance as a function of the disk luminance in the steady and flashed conditions (data for a representative subject among three). The luminance value matched with phosphenes on the dark background is slightly above the "dimmer" value of the disk. On the diagonal gray line, the matched luminance is equal to the disk luminance. Therefore, the matched luminance above (below) the gray line indicates the brightening (darkening) effect by paired-pulse TMS. In the steady displays, the phosphene region appeared darker in the "brighter" disk (t-test on the difference from the disk luminance, $p < .01$ for all subjects), while it appeared brighter in the "dimmer" disk ($p < .01$). In the flashed displays, on the other hand, the phosphene region was reported to be brighter in both the "dimmer" and "brighter" disks ($p < .01$).

The brightness reduction in the steady "brighter" display clearly indicates that the effect of paired-pulse TMS can not be considered as a mere addition of brightness. The brightness in the phosphene region of the steady disk seems to be drawn toward the brightness of the phosphene on the dark background, although more systematic manipulation of the disk luminance will be needed to determine at which disk luminance the effect switches from brightening to darkening.

The results in the flashed displays may be regarded as an addition of brightness. However, it is not clear whether it is a result of addition of a phosphene with some constant brightness and color regardless of the background, or enhancement of the existing signals

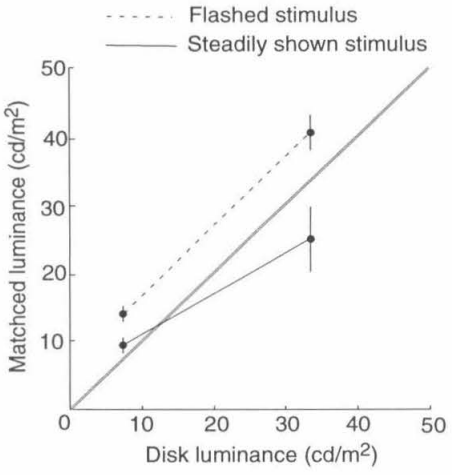

Figure 5.6: Brightness modulation by paired-pulse TMS
The luminance matched to the brightness in the phosphene region is plotted against the disk luminance for a representative subject. The solid and dotted lines show the results of the steady and flashed disks, respectively. The error bar represents standard deviation. On the diagonal gray line, the matched luminance is equal to the disk luminance.

in the background. This issue may be resolved by using visual stimuli with additional attributes such as color and texture: for example, a colored disk should change its color due to the addition of a phosphene of a different color, while the enhancement of the background should result in the same color (hue) but higher brightness.

Although paired-pulse TMS leads to quite different perceptual effects from those induced by single-pulse TMS, they are common in that the resulting percepts reflect interactions with visual inputs, especially with the temporal attributes of them. Further studies will be required to characterize the effects of paired-pulse TMS on visual perception in terms of the timing between magnetic pulses and visual stimuli, as well as the spatial interactions between them.

Part II

Biophysics (Chapter 6–8)

Chapter 6 Modeling magnetic stimulation: An overview

Despite a vast amount of reports on behavioral and cognitive effects of TMS, its biophysical mechanisms are poorly understood. Furthermore, little physiological data are available on how single neurons in the brain respond to magnetic stimulation.

Modeling may be a powerful method to study the biophysics of magnetic stimulation, since the physics of this technique can be described in a mathematically rigorous manner, and it could be combined with neural modeling methods used in computational neuroscience. Modeling of magnetic stimulation is of great importance in interpreting perceptual or behavioral effects of TMS in terms of neural electrical activity. Furthermore, predictions from the modeling may allow us to design new TMS experiments and effective instrumentation.

Modeling of magnetic stimulation consists of different levels, including the macroscopic distribution of electromagnetic fields, as well as the microscopic behavior of charged ions that affects the neuronal membrane potential. In the following sections of this chapter, we review basic physical and biophysical principles of magnetic stimulation, and describe the goals of our realistic neuron model.

6.1 Magnetic stimulator

The magnetic stimulator can be modeled by a series RLC circuit (Roth & Basser, 1990) as shown in Figure 6.1a. The current pulse is generated when a capacitor C, initially charged to a voltage V_0, is discharged through a coil with an inductance L and a resistance R. In practice, the circuit may be more complex, containing, for example, several capacitors wired in parallel, a transformer to increase the current in the coil, or nonlinear elements such as diodes to reduce oscillations (Cohen, 1985; Polson *et al.*, 1982; Barker *et al.*, 1987; Bickford *et al.*, 1987). We use this circuit for the description of basic principles of TMS and for our simulation, since it is the simplest model of a stimulator that produces realistic current waveforms.

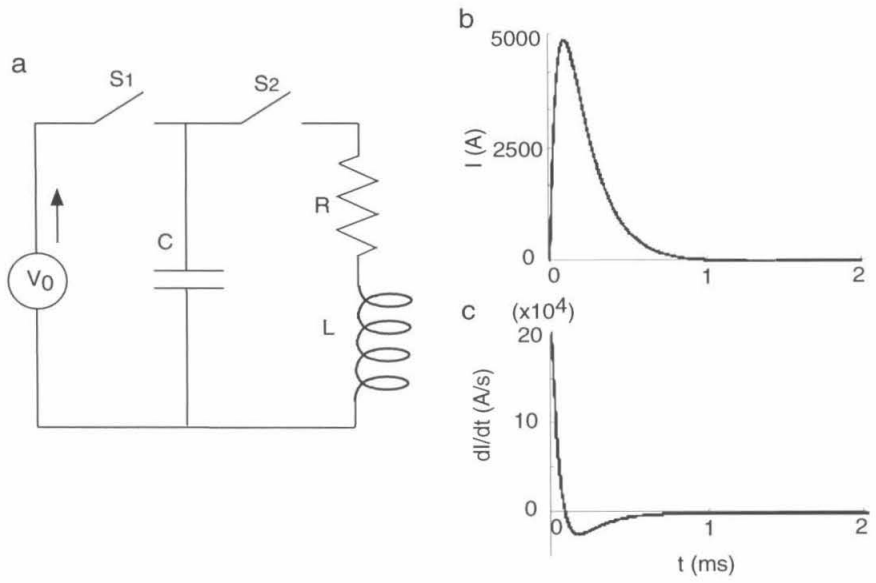

Figure 6.1: Magnetic stimulator
(a) Stimulator circuit. The capacitor C is charged to an initial potential V_0 by closing the switch S_1. The capacitor is discharged through the coil with an inductance L and a resistance R by closing S_2. (b) Time course of the current in the coil. The current is calculated by Equation 6.2. (c) Time derivative of the coil current. The induced electric field is proportional to the time derivative of the coil current.

The inductance L of a circular coil of a radius r_c wound with N turns of wire having a radius r_w is (Smythe, 1968)

$$L = \mu_0 r_c N^2 \left(\ln \left(\frac{8 r_c}{r_w} \right) - 1.75 \right) \tag{6.1}$$

where μ_0 is the magnetic permeability of air ($4\pi \times 10^{-7}$ N/A^2). Using this value L, and given C, R, and V_o, we derive the coil current $I(t)$, where t is the time from the discharge, according to elementary circuit theory. The current either rises to a maximum and then falls to zero (overdamped), or oscillates with decreasing amplitude (underdamped), depending on whether $R^2/(4L^2) - 1/(LC)$ is greater than or less than zero, respectively (Geddes, 1988). If the circuit is overdamped, the current is given by

$$I(t) = V_0 C \omega_2 e^{\omega_1 t} \left(\left(\frac{\omega_1}{\omega_2} \right)^2 - 1 \right) \sinh(\omega_2 t) \tag{6.2}$$

where

$$\omega_1 = \frac{R}{2L} \tag{6.3}$$

and

$$\omega_2 = \sqrt{\left(\frac{R}{2L} \right)^2 - \frac{1}{LC}}. \tag{6.4}$$

If the current is underdamped,

$$I(t) = V_0 C \omega_2 e^{\omega_1 t} \left(\left(\frac{\omega_1}{\omega_2} \right)^2 + 1 \right) \sinh(\omega_2 t) \tag{6.5}$$

where ω_1 is the same as given above and

$$\omega_2 = \sqrt{\frac{1}{LC} - \left(\frac{R}{2L} \right)^2}. \tag{6.6}$$

The overdamped current is referred to as a monophasic pulse in the TMS literature. It is generally preferred, as the induced electric field, whose amplitude is proportional to the the time derivative of the coil current, can be made selective for its direction, provided that the resistance and capacitance are adjusted such that the coil current rises faster than it falls. In our psychophysical experiments, we used a stimulator that produce monophasic pulses (Magstim 200).

Figure 6.1b shows the waveform obtained with $N = 15$ turns, r_c (coil radius) = 3.5 cm, r_w (wire radius) = 1 mm, $V_0 = 6000$ V, $C = 200$ μF, and $R = 1$ Ω. Figure 6.1c depicts the time derivative of the coil current. The coil parameters were chosen to be similar to those we used in our psychological studies. The circuit parameters were adjusted to approximate the waveform of our stimulator.

6.2 Electric field induced by a changing magnetic field

To derive the magnetic and electric fields induced by the magnetic stimulator, we make "quasistatic" assumptions, thereby ignoring the effects of electromagnetic wave propagation (Plonsey & Heppner, 1967). The first assumption is to neglect the wave length of electromagnetic waves. At the frequencies of interest in TMS (up to 10 kHz, corresponding to a 100 μs rise time of the pulse current), the wavelength of electromagnetic radiation is on the order of kilometers, which is much longer than any distance associated with the human body, thus can be neglected in bioelectric calculations (Sullivan *et al.*, 1987).

Second, we can neglect the attenuation of electromagnetic fields due to the induced currents in the tissue. The induced currents in the tissue produce their own magnetic fields that tend to cancel out the applied fields. This cancellation becomes more complete with depth into the tissue. The depth at which the magnetic field in the tissue is approximately one-third of the external field is called the skin depth δ. It depends on the frequency of the wave f, the conductivity of the tissue σ, and the magnetic permeability of the tissue μ,

$$\delta = \sqrt{\frac{1}{\mu\pi\delta f}}. \tag{6.7}$$

Given a frequency of 10 kHz (corresponding to a 100 μs rise time), a conductivity of 1 S/m (Foster & Schwan, 1989), and a permeability of 4π x 10^{-7} N/A^2 (equal to that of air), the skin depth is approximately 5 m, which is large compared to the size of commonly used magnetic coils (several centimeters in diameter). Thus, the attenuation of the magnetic field due to induced currents can be neglected in TMS.

Under these assumptions, the magnetic vector potential induced by the coil current $I(t)$

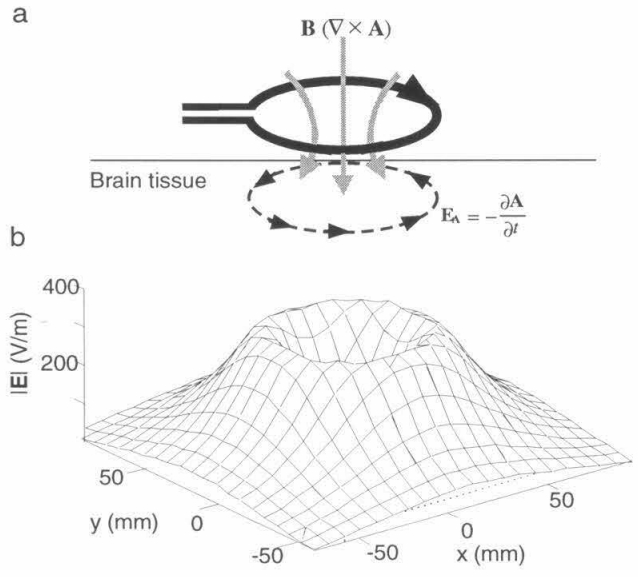

Figure 6.2: Induced electric field
(a) The current in the coil (black line) produces a magnetic field (gray lines). The time-varying magnetic field induces an electric field (dotted line). (b) The amplitude of the electric field induced by a circular coil 10 μs after the discharge is plotted. The electric field was calculated in the plane 1.5 cm below and parallel to the coil, using the same parameters as in Figure 6.1. The circular coil was approximated as a 128-sided polygon, and the integral in Equation 6.10 was numerically solved as the sum of the contributions of the sides.

at a position $\mathbf{r}$ and a time t is calculated by (Cohen *et al.*, 1990)

$$\mathbf{A}(\mathbf{r},t) = \frac{\mu_0 N I(t)}{4\pi} \int \frac{d\mathbf{l}'}{|\mathbf{r}-\mathbf{r}'|} \tag{6.8}$$

where N is the number of turns in the coil, $d\mathbf{l}$' is a vector representing a small length of the coil (pointing in the direction of the current), and $\mathbf{r}$' is a vector indicating the position of $d\mathbf{l}$'. The magnetic field is, by the definition of the vector potential (Jackson, 1975),

$$\mathbf{B}(\mathbf{r},t) = \nabla \times \mathbf{A} = \frac{\mu_0 N I(t)}{4\pi} \nabla \times \int \frac{d\mathbf{l}'}{|\mathbf{r}-\mathbf{r}'|}. \tag{6.9}$$

The electric field due to magnetic induction is the negative of the time derivative of $\mathbf{A}$ (Jackson, 1975)

$$\mathbf{E_A}(\mathbf{r},t) = -\frac{\partial \mathbf{A}}{\partial t} = -\frac{\mu_0 N}{4\pi} \frac{\partial I(t)}{\partial t} \int \frac{d\mathbf{l}'}{|\mathbf{r}-\mathbf{r}'|}. \tag{6.10}$$

The induced electric field is expressed as the product of the time-dependent component $(dI(t)/dt)$ and the space-dependent component (the integral). Hence, the spatial distribution pattern of the electric field is time-invariant, while the temporal profile of the amplitude is identical at any position, being proportional to the time derivative of the current in the coil as shown in Figure 6.1c. If the coil is flat, the induced electric field at any position is parallel to the plane of the coil, since $d\mathbf{l}'/|\mathbf{r}\text{-}\mathbf{r}'|$, which is integrated to determine the direction of the electric field, is always parallel to the plane of the coil. Figure 6.2a illustrates schematically the electromagnetic induction by a coil. Figure 6.2b plots the amplitude of the electric field induced in a plane parallel to the coil (using the same parameters as in Figure 6.1). We note that the electric field is induced along the loop of the coil, and peaks just below the loop, not at the center of the coil.

6.3 Two sources of electric field

An electric field generally has two sources: changing magnetic fields and charge distribution. The total electric field is the sum of the fields due to magnetic induction and electric charges (Jackson, 1975)

$$\mathbf{E_{total}} = -\frac{\partial \mathbf{A}}{\partial t} - \nabla \Phi \tag{6.11}$$

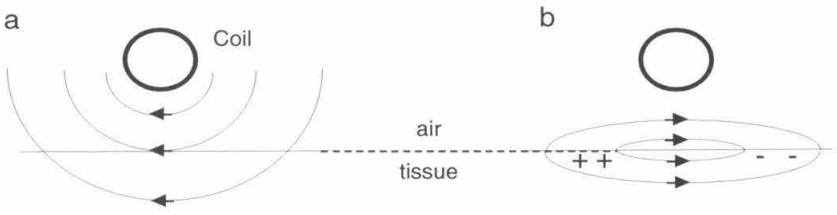

Figure 6.3: Two sources of electric field
(a) The induced electric field by the coil placed perpendicular to the surface of the tissue is displayed. The electric field is not distorted at the border, because there is little difference in magnetic permeability between air and biological tissues. (b) The electric field due to magnetic induction (a) causes a current flow in the tissue, resulting in charge accumulation at the border (+ and −). The total electric field is the sum of those in (a) and (b). Adapted from Roth *et al.* (1991).

where Φ is the scalar potential, or simply the voltage, determined by the charge distribution. The first term, due to magnetic induction, is identical to $\mathbf{E_A}$ shown in Equation 6.10. The second term, due to electric charges, is of significant importance in electrophysiology, as the electric signals in normally functioning neurons are constituted by charged ions such as Na^+ and K^+.

In calculating the electric field in the brain induced by TMS, it is important to consider the charge accumulation caused by magnetic induction. Figure 6.3 illustrates the effect of magnetic stimulation on charge distribution at the boundary between air and a brain tissue (Roth *et al.*, 1991). When a circular coil in the air is oriented perpendicular to the flat surface of the tissue, the induced electric field penetrates the tissue, forming concentric loops as shown in Figure 6.3a. Positively charged ions in the tissue move in the direction of this electric field, and negatively charged ions in the opposite direction, until they reach the surface of the tissue. This movement of charges produces an additional electric field as shown in Figure 6.3b. The total electric field is the sum of these electric fields, one due to magnetic induction and the other due to charge accumulation. Charges accumulate until the component of the total electric field perpendicular to the tissue surface becomes zero (Jackson, 1975).

Any conductivity changes along the path of the induced electric field, not only at the boundary between air and a tissue, cause nonuniformity of electric charges. To calculate the electric field distribution in brain-like structures, Equation 6.10 has been analytically

solved for magnetic stimulation of simple volume conductor models such as semi-infinite space (Durand *et al.*, 1992), spheres (Eaton, 1992), and infinite-length cylinders (Esselle & Stuchly, 1994). For other shapes and inhomogeneous objects, Equation 6.10 has been numerically solved (Ueno *et al.*, 1988; Saypol *et al.*, 1991). These models have provided valuable information as to the macroscopic locus of stimulation in the brain.

6.4 Cable model

At the microscopic level, the electric field due to magnetic induction sets free charges into coherent motion both in the intra- and extracellular spaces. This motion and the intervention of it by the cell membrane lead to depolarization or hyperpolarization of the membrane potential. The currents due to magnetic induction (eddy currents) may not be the only source of the neural stimulation. However, other mechanisms, such as those responsive to static magnetic fields, have not been identified (Ueno, 1994).

Roth & Basser (1990) first studied the effect of the magnetically induced currents on the membrane potential using a cable model. Basic assumptions they made are: 1) the membrane potential is only a function of the axial variable, 2) the axoplasm behaves like a linear Ohmic conductor, 3) the extracellular potential produced by the fiber's own activity is negligible (Rattay, 1986), and 4) the extracellular medium is electrically grounded. Under these assumptions, the behavior of the transmembrane potential V in a passive cable with infinite length and fixed axial and membrane resistances can be described by the cable equation

$$\lambda^2 \frac{\partial^2 V}{\partial x^2} - \tau \frac{\partial V}{\partial t} - V = \lambda^2 \frac{\partial E_i}{\partial x} \tag{6.12}$$

where E_i is the axial component of the induced electric field $\mathbf{E_A}$, and λ and τ are the space and time constants, respectively. The coordinate x measures the distance along the fiber. This equation can be obtained by simply replacing the axial current in the derivation of the ordinary cable equation (Rall, 1989)

$$i_i = -\frac{1}{r_i} \frac{\partial V}{\partial x} \tag{6.13}$$

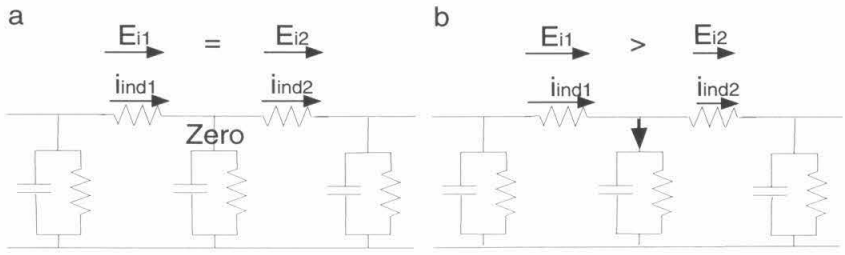

Figure 6.4: Cable model of magnetic stimulation
The membrane is represented by a set of discrete isopotential R-C components. The upper and lower sides are the intra- and extracellular spaces, respectively. E_{i1} and E_{i2} are the axial components of the induced electric field at adjacent portions of the cable. i_{ind1} and i_{ind2} are the induced axial currents due to E_{i1} and E_{i2}, respectively.

where r_i is the axial resistance per unit length, with

$$i_i = -\frac{1}{r_i}\frac{\partial V}{\partial x} + \frac{E_i}{r_i}. \tag{6.14}$$

E_i/r_i represents the induced current in the fiber due to magnetic induction. The new term in the cable equation (6.12) with E_i acts like a sink of transmembrane potential, with a strength proportional to the axial derivative of the induced electric field.

Figure 6.4 illustrates how axial derivative of the induced electric field contributes to the membrane potential. When there is no difference in the induced electric field between adjacent portions of the fiber (Figure 6.4a), the same amount of currents are induced in these portions, thus the current flows along the fiber without contributing to the membrane potential. When there is a spatial gradient in the induced electric field (Figure 6.4b), the difference of the induced currents is diverted into the membrane current, causing a change in the membrane potential.

Roth & Basser (1990) demonstrated that an action potential can be generated by magnetic stimulation of a straight and uniform cable model of infinite length with Hodgkin-Huxley-type voltage dependent channels. The site of the initiation of an action potential was shown to be close to the negative peak of the axial derivative of the induced electric field as predicted from the cable equation. This was also experimentally confirmed in peripheral nerves *in vitro* (Maccabee *et al.*, 1993).

Although this cable model seems to capture essential features of magnetic stimulation of neural fibers, the underlying assumptions may not be always valid. The assumption of the extracellular medium being electrically grounded is only true in the case of an isolated fiber located in an infinite homogeneous conducting medium (Basser *et al.*, 1992). Nagarajan & Durand (1996) extended the cable equation in the case of inhomogeneous extracellular space, where the axial gradient of the extracellular potential needs to be incorporated as an additional term. However, it is difficult to model the distribution of extracellular potential caused by the inhomogeneity of the brain tissue.

Another remark on the previous assumption is that the membrane potential may depend on factors other than axial variables. The induced electric field transverse to the fiber is known to contribute to neural excitation (Krassowska & Neu, 1994; Roth, 1994; Ruohonen *et al.*, 1996). The transverse electric field depolarizes one side of the membrane, and hyperpolarizes the other side. In the presence of voltage-dependent channels, the depolarization of only one side of the membrane could lead to an action potential. However, the effect of the transverse field is estimated to be small, especially for cortical neural fibers with small diameters (Ruohonen *et al.*, 1996).

6.5 Magnetic stimulation of cortical neurons: A perspective

Among the various levels of modeling we have presented so far, the microscopic level concerned with the neuronal membrane potential seems crucial in understanding neural responses to TMS and their relation to perception and behavior. With the cable model and its compartmental form, it has been demonstrated that the brief magnetic pulse typically used in TMS can generate an action potential in a straight axonal model or in a simplified neuron model with an active soma and a few straight passive dendrites (Roth & Basser, 1990; Nagarajan *et al.*, 1993). Although these models explain the behavior of a peripheral nerve under magnetic stimulation, more elaborate modeling strategy seems to be required to account for basic aspects of the effects of TMS.

For instance, as we have shown in Part I, a single magnetic pulse (duration, 1 ms) applied to the occipital lobe typically causes inhibitory effects on visual perception. The inhibition seems to last at least for tens of milliseconds, since visual stimuli of a 40-80 ms duration can be made nearly invisible, and the stimulation was effective over a wide range

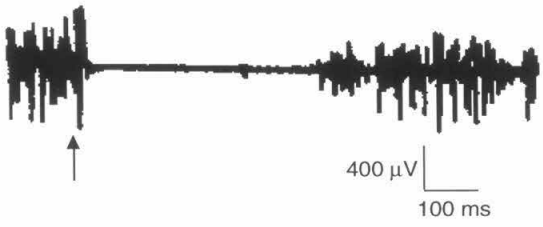

Figure 6.5: EMG during voluntary muscle contraction
A single magnetic pulse, whose timing is indicated by an arrow, was applied to the motor cortex during muscle contraction. The magnetic pulse produced motor evoked potentials (the higher amplitudes immediately following the magnetic pulse) followed by a long silent period. From Inghilleri *et al.* (1993) with permission.

(approximately 100 ms) of the delay from the flashed visual stimuli. Similarly, TMS of the motor cortex generally causes long inhibitory effects (Hallett, 1995), though the muscle activation is more apparent and well documented. Figure 6.5 shows an electromyographic (EMG) recording obtained when a magnetic pulse was applied over the motor cortex during voluntary muscle contraction (Inghilleri *et al.*, 1993). The initial brief activation is followed by a long inhibitory period of over 100 ms. It is also known that the inhibition is present even with low intensity of TMS that can not induce muscle activation (Hallett, 1995). Thus, substantially longer inhibition compared with the stimulating pulse duration is a ubiquitous and general feature of of the brain stimulation. The previous axonal models, however, only demonstrate the generation of one or a few action potentials in a time scale comparable to that of the stimulating magnetic pulse, and thus fail to explain the fundamental aspect of the effects of TMS.

To understand neural responses to TMS pertinent to its perceptual or behavioral effects, we need biophysically and morphologically realistic models of neurons and their network. As a first step, we created a compartmental model of single cortical neurons under magnetic stimulation. We extended the cable model described above, adopting the assumptions made by Roth & Basser (1990); namely, the model neuron was assumed to be placed in an infinite homogeneous conducting medium, and the transverse component of the induced electric field was neglected. In Chapter 7, we present a mathematical theory to derive the effect of the induced electric field on a neuron of arbitrary structure. In addition, methods for computer simulation are described in which the effect of the induced electric field is

integrated with a realistic multicompartmental model of cortical neurons. In Chapter 8, we show simulation results of the realistic cortical neuron model with magnetic stimulation, which exhibit behavior pertinent macroscopic effects of TMS. The relation to our psychophysical results is also discussed.

Chapter 7 Modeling magnetic stimulation of cortical neurons

7.1 Transmembrane current induced by magnetic stimulation

Cortical neurons are composed of extensively arborized fibers with numerous bends and changing diameter. In such complex structure, the stimulation due to magnetic induction can occur in a manner quite different from that of straight and uniform fibers of infinite length. As we have discussed in the previous chapter, the spatial gradient of the induced electric field causes additional transmembrane currents leading to the stimulation in straight fibers (Figure 7.1a). However, transmembrane currents are produced wherever the induced axial currents vary along the current path, not only due to the spatial gradient of the electric field itself. Even under a spatially uniform electric field, the induced axial currents change at neuronal bends because of the difference in the axial projections of the electric field, resulting in transmembrane currents (Figure 7.1b). Since the induced axial current is a function of the axial resistance, which typically depends on the diameter of the fiber, a transmembrane current arises where the axial resistance or the diameter changes (Figure 7.1c). Furthermore, an axial current flowing toward (away from) the end of the fiber can be regarded as a positive (negative) transmembrane current (Figure 7.1d). At branching points, the difference between the currents flowing into and those flowing away from them contributes as a transmembrane current (Figure 7.1e). These factors of stimulation have been stated or partially modeled (Roth & Basser, 1990; Nagarajan *et al.*,1993; Maccabee *et al.*, 1993; Amassian, 1994), but have not been integrated within a general and efficient method applicable to arbitrary neuronal structure.

In theory, magnetic stimulation of a neuron can be simulated by injecting the above transmembrane currents into a neuron model with cable properties and membrane channel mechanisms as well as structural information. Realistic neuron models have been developed using the multicompartmental method, where the membrane properties of a short neural

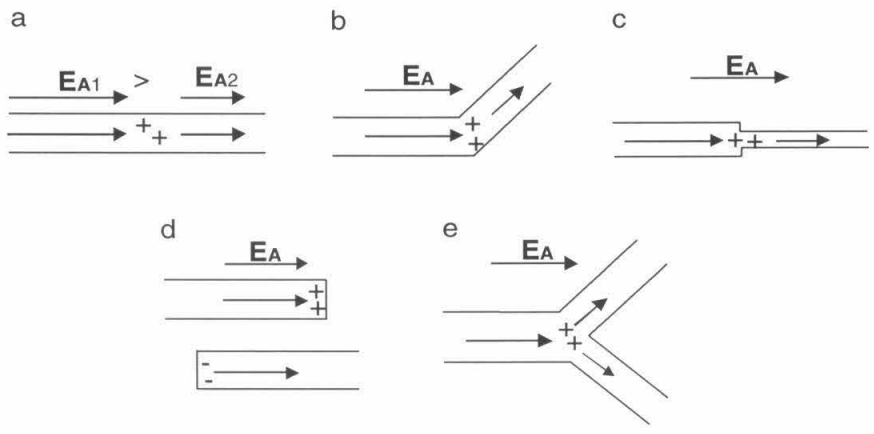

Figure 7.1: Sites of transmembrane currents due to magnetic induction
$\mathbf{E_A}$ represents an electric field due to magnetic induction. The arrows inside the cables are the induced axial currents, and + and - stands for positive and negative charges contributing as transmembrane currents, respectively. Transmembrane currents are induced where the electric field is spatially nonuniform (a), the fiber bends (b), the axial resistance (diameter) changes (c), the fiber ends (d), and the fiber branches (e).

segment are approximated by an isopotential electrical compartment, and such compartments are connected to simulate the overall behavior of the membrane potential (Segev & Burke, 1998). The three-dimensional structure of neurons have been microscopically reconstructed by recording the three-dimensional position and the diameter of discrete points along the fibers (Douglas *et al.*, 1991; Mainen & Sejnowski, 1996; Paré *et al.*, 1998). Three-dimensional reconstruction is available in finer resolution than the size of compartments used in relatively high resolution models (on the order of 10 μm; Segev & Burke, 1998).

However, it is not practical to calculate a current at every point where the induced axial current changes, since the current nonuniformity does not alway occur at discrete points, but can spread continuously due to the continuous changes in neuronal structure. Even if discrete structural information is used, the calculation of the currents becomes computationally intractable with higher resolutions of the reconstruction.

In building a multicompartmental model of a complex neuron, we calculate the total transmembrane current into each neural segment from which a single compartment is created. Then, the total current is injected into each compartment to simulate the effect of magnetic stimulation. The currents at the ends and the branching points are also incorpo-

rated in our model. In the following section, we develop a theory to calculate these currents accurately and efficiently for any given neuronal structure. Our method will be compared with another method used to build a compartmental model of simple neuronal structure (Nagarajan *et al.*, 1993).

7.2 Theory for complex neuronal structure

7.2.1 Current injection in a compartmental model

The axial component of an induced electric field, which produces an axial current flow in a neuronal fiber, is given by

$$E_i(x) = \mathbf{E_A}(\mathbf{r}(x)) \cdot \mathbf{s}(x) \tag{7.1}$$

where $\mathbf{E_A}$ is the induced electric field as calculated by Equation 6.10, and x is the position along the fiber. In arborized neurons, we measure the position x for each branch independently. The position of one of the terminals in each unbranched fiber is termed the "starting" position or x_s, and that of the other terminal is termed the "ending" position or x_e. x_s and x_e can be arbitrarily determined for each fiber. $\mathbf{r}(x)$ represents the coordinate transformation from the relative position in the fiber to the Cartesian space. $\mathbf{s}(x)$ is a unit vector indicating the direction of the fiber at x, pointing toward x_e. The axial component leads to current induction along the fiber according to the Ohmic property of the axoplasm

$$i_{ind}(x) = \frac{E_i(x)}{r_i(x)} = \frac{\mathbf{E_A}(\mathbf{r}(x)) \cdot \mathbf{s}(x)}{r_i(x)} \tag{7.2}$$

where $r_i(x)$ is the axial resistance of the fiber at x. Note that we treat the axial resistance as a function of the position unlike in Equation 6.12 (the cable equation). Here, we assume that the axial resistance r_i and the direction of the fiber $\mathbf{s}$ are given for continuous points x. The method used to calculated these values from the discrete data of neuronal reconstruction is described in Section 7.3.2.

The density of the transmembrane current due to the nonuniformity of current induction is derived by taking the negative of the spatial derivative of the above axial current i_{ind},

$$i_{tr}(x) = -\frac{\partial i_{ind}(x)}{\partial x} = -\frac{\partial}{\partial x}\left(\frac{\mathbf{E_A}(\mathbf{r}(x)) \cdot \mathbf{s}(x)}{ri(x)}\right). \tag{7.3}$$

As noted from this formula, the transmembrane current depends on the spatial distribution of the induced electric field ($\mathbf{E_A}$; Figure 7.1a), the direction of the fiber ($\mathbf{s}$; Figure 7.1b), and the axial resistance, which is typically dependent on the diameter of the fiber (r_i; Figure 7.1c).

Suppose we create a compartment from a segment $[x_0, x_1]$ of a fiber, the total transmembrane current induced in the segment, which is injected into the compartment, is calculated by

$$\begin{aligned} I_{seg[x_0,x_1]} &= \int_{x_0}^{x_1} i_{tr}(x)dx \\ &= \int_{x_0}^{x_1} -\frac{\partial i_{ind}(x)}{\partial x}dx \\ &= i_{ind}(x_0) - i_{ind}(x_1). \end{aligned} \tag{7.4}$$

Note that the total transmembrane current in the segment is determined by the induced currents at x_0 and x_1, which depend only on the electric field and the neuronal structure at these points, as indicated in Equation 7.2. This allows us to accurately and efficiently calculate the total membrane current within a segment regardless of the geometrical complexity.

Assuming that neuronal terminals are sealed, no current flows through the high impedance of the terminal membrane, thus the induced axial currents flowing toward (away from) them result in the equivalent amount of positive (negative) transmembrane currents (Nagarajan *et al.*, 1993). In our formulation, the sign of the induced current depends on the choice of x_s and x_e in each fiber (Equation 7.2). Hence, we express the transmembrane currents separately for neuronal terminals which are defined as x_s and for those defined as x_e

$$I_{ter} = \begin{cases} -i_{ind}(x_{ter}) & \text{if } x_{ter} = x_s \\ i_{ind}(x_{ter}) & \text{if } x_{ter} = x_e \end{cases} \tag{7.5}$$

where x_{ter} is the position of the terminal in the fiber.

At branching points, magnetic stimulation leads to a transmembrane current equivalent to the difference between the axial currents flowing into them and those away from them. Considering the sign of currents as before, the transmembrane current at a branching point

is

$$I_{br} = \sum_{m \in F_s} -i_{ind}(x_{br}(m)) + \sum_{m \in F_e} i_{ind}(x_{br}(m)) \tag{7.6}$$

where m is the index for the fiber converging to the branching point. F_s and F_e are the sets of the indices for the fibers "starting" and "ending" at the branching point, respectively. $x_{br}(m)$ is the relative position of the branching point in the fiber m.

These currents are injected into the compartmental model as illustrated in Figure 7.2. Note that nonuniformity of the induced electric field, neuronal bends, and axial resistance (diameter) changes as indicated in Figure 7.1a, b, and c are all incorporated in Figure 7.2a.

Nagarajan *et al.* (1993) simulated the effect of magnetic stimulation on a straight axonal cable of finite length, using a compartmental model. They injected a current into each compartment equivalent to the difference between the mean axial currents in adjacent neuronal segments. Even though this is a valid method to approximate the transmembrane currents due to magnetic induction, the calculation of the mean axial current in a segment requires the information on the geometry of the fiber and the electric field at every point within the segment, unlike the calculation of the total transmembrane current employed in our model. Therefore, it is practically impossible to apply their method to complex neuronal structure.

7.2.2 Total current in a whole neuron

The theory given above enables us to characterize the overall nature of transmembrane currents due to magnetic induction in a whole neuron. The total current in a non-arborized neural fiber is the sum of the total current into the "segment" starting and ending at the terminals of the fiber, and the currents at the terminals

$$\begin{aligned} I_{total} &= I_{seg[x_s,x_e]} + I_{ter(x_s)} + I_{ter(x_e)} \\ &= i_{ind}(x_s) - i_{ind}(x_e) - i_{ind}(x_s) + i_{ind}(x_e) \\ &= 0. \end{aligned} \tag{7.7}$$

Interestingly, the total amount of current injected into a non-arborized fiber is zero at any moment regardless of the complexity of the neuronal and electric field geometry.

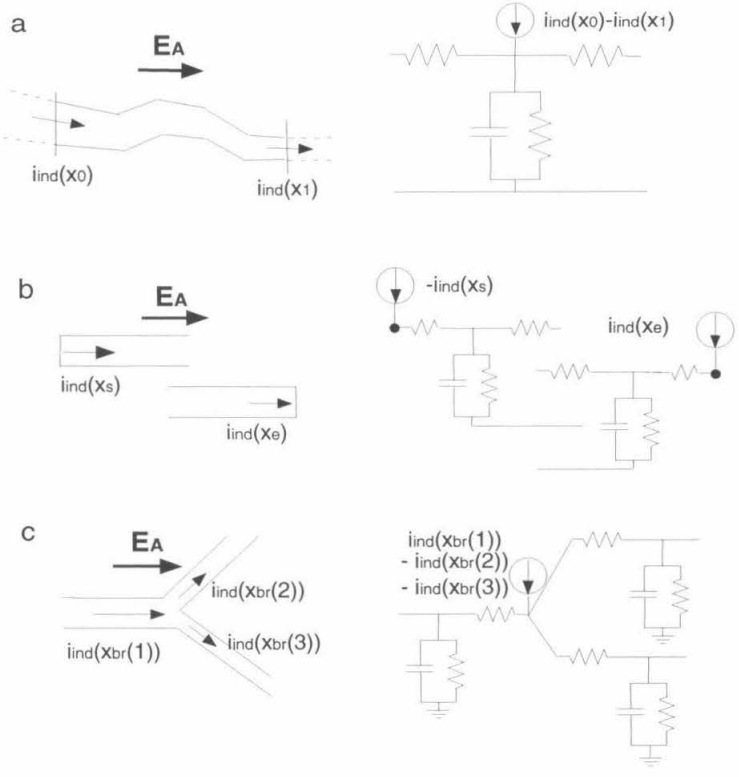

Figure 7.2: Implementation of magnetic stimulation in a compartmental model
The effect of magnetic stimulation is modeled by injecting currents for neuronal segments (a), terminals (b), and branching points (c). The left column shows neuronal structures with an induced electric field ($\mathbf{E_A}$) and the induced axial currents (arrows inside the cables). The right column shows electric circuits representing parts of the compartmental model incorporating the effect of magnetic stimulation. The pairs of a capacitor and a resistor indicate isopotential compartments, and the resistors connecting them are axial resistances. The arrows and the circles show current injection points.

This can be extended to arborized neuronal structure. By comparing Equations 7.5 and 7.6, we can see that the transmembrane current at a branching point is identical to the sum of the terminal transmembrane currents obtained when the converging fibers are considered separately, as if disconnected at the branching point

$$I_{br} = \sum_{m \in F} I_{ter}(m) \tag{7.8}$$

where F is the set of the indices for all the fibers converging to the branching point. $I_{ter}(m)$ is the transmembrane current at the disconnected terminal of the fiber m. Therefore, the total amount of current injection in an arborized neuron is identical to the sum of currents in the disconnected branches that constitute the neuron. Since the total transmembrane current in each disconnected branch is zero (Equation 7.7), the sum of the contributions of the branches is also zero. Hence, the total amount of current injection in an entire neuron of arbitrary structure including arborization is zero at any moment. It is equivalent to stating that the charge in the intracellular space is conserved during magnetic stimulation.

7.2.3 Neuronal size and effectiveness of stimulation

The analysis of the total transmembrane current given above implies that even when positive transmembrane currents are locally generated, they are accompanied by negative currents at other locations to balance them. In small neurons, positive and negative injected currents, which tend to be closely spaced, are likely to be canceled out without causing any significant effect on the local membrane potential. Figure 7.3 illustrates the effect of neuronal size on the effectiveness of stimulation using a straight and uniform passive cable with sealed ends, under a steadily applied, uniform electric field. The electric field $\mathbf{E_A}$ induces the positive and negative transmembrane currents of the same amplitude at the terminals (i_{ind} and $-i_{ind}$), which can be regarded as current injection at these points. The steady state membrane potential V is solved by linearly combining the solutions for current injection at single terminals (Koch, 1999)

$$\frac{V(X)}{V_{0,L}} = \frac{-\cosh(L-X) + \cosh(X)}{\cosh(L)} \tag{7.9}$$

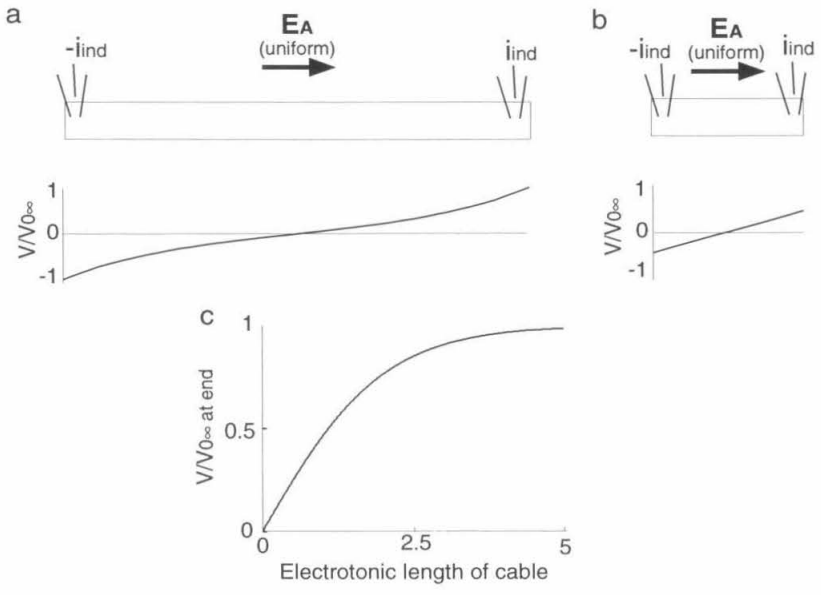

Figure 7.3: Neuronal size and effectiveness of stimulation
(a, b) A straight passive cable with a uniform axial resistance and sealed ends is stimulated by a uniform electric field ($\mathbf{E_A}$), resulting in transmembrane current at the terminals (i_{ind} and $-i_{ind}$). The normalized steady state potential ($V/V_{0,\infty}$) is shown as a function of the position in the cable. The electrotonic length of the cable in (a) is 4, while that in (b) is 1. (c) The normalized steady state potential at the terminal is plotted as a function of the electrotonic length of the cable.

where X and L are are the position and the cable length in electrotonic units (length normalized with the space constant of the cable), respectively. $V_{0,L}$ represents the steady state potential at the injection point obtained when the positive current i_{ind} is applied into only one of the terminals. $V_{0,L}$ depends with the cable length L

$$V_{0,L} = V_{0,\infty} \coth(L) \tag{7.10}$$

where $V_{0,\infty}$ is the steady state potential at the injection point of a semi-finite cable obtained when the same current i_{ind} is applied to the origin of the cable. This formula can be derived from the relation between the input resistance of the finite cable R_L and that of the semi-finite cable R_∞ (Koch, 1999)

$$R_L = R_\infty \coth(L). \tag{7.11}$$

By substituting Equation 7.10 into Equation 7.9, we obtain the the steady state potential normalized by $V_{0,\infty}$, which does not depend on the cable length L

$$\frac{V(X)}{V_{0,\infty}} = \frac{-\cosh(L-X) + \cosh(X)}{\sinh(L)}. \tag{7.12}$$

Figure 7.3a and b illustrate the solutions for long ($L = 4$) and short ($L = 1$) cables. Compared to the long cable (a), the shorter cable (b) exhibits substantial cancellation of the positive and negative currents. The normalized potential at the terminal $X = L$ is given by

$$\frac{V(L)}{V_{0,\infty}} = \frac{\cosh(L) - 1}{\sinh(L)}. \tag{7.13}$$

This formula can be regarded as a function of L, indicating the effect of the cable length on the effectiveness of stimulation (Figure 7.3c). Since even major trunks of cortical pyramidal neurons have electrotonic length of less than one (Zador *et al.*, 1995), the steep slope at the cable length of 0-2 in Figure 7.3c suggests that the size critically affect the strength of stimulation in cortical neurons. For better estimation of the overall effectiveness of stimulation, however, the transient state as well as the structural complexity will need to be analyzed.

7.3 Computational methods

We modeled magnetic stimulation of cortical neurons by combining standard compartmental modeling techniques and the current injection equivalent to magnetic stimulation discussed in the previous section. The cortical neuron model was taken and modified from Mainen & Sejnowski (1996). The channel dynamics and the model parameters were not modified except that a shorter integration time step and smaller compartment sizes were used. We used their neuron model since it is simple but able to produce a variety of intrinsic firing patterns observed in actual cortical neurons. Simulations were performed in the NEURON (Hines, 1993) environment. The neuron model and the method used to simulate magnetic stimulation on it are detailed below.

7.3.1 Neuron model

The cortical neuron model has a low density of Na^+ channels in the soma and dendrites (Stuart & Sakmann, 1994), and a high density in the axon hillock and initial segment (Wollner & Catterall, 1986). Fast K^+ channels were present in the axon and soma, while slow voltage- and Ca^{2+}-dependent K^+ channels were in the soma and dendrites (Schwindt *et al.*, 1988; Storm, 1990), along with high-threshold Ca^{2+} channels. The currents through these channels were calculated with conventional Hodgkin-Huxley-type kinetics with an integration time step of 10 μs. The specific equations for these currents are given in the Appendix.

Digital reconstructions of neocortical neurons (Layer 5 pyramid, Layer 3 pyramid, and Layer 3 aspiny stellate; Figure 7.4) were obtained from the literature (Hines, 1993; Mainen & Sejnowski, 1996). The data contained the discrete positions of the dendritic branches and soma, and the diameter at each position. An axon, which was not present in the reconstructed anatomy, was attached to the soma of each cell. The axon consisted of a conical hillock (10 μm long), tapering to one-quarter width to a cylindrical initial segment region (15 μm) followed by 5 myelinated internodes (100 μm) separated by nodal segments (Mainen *et al.*, 1995). All dendritic branches, soma, and axon were divided into cylindrical compartments with a maximum length of 10 μm. Compartmentalization with a shorter maximum length (5μm) yielded similar results. The dendritic membrane area of the pyramidal cells was increased to account for spines, which were not given in the reconstruction

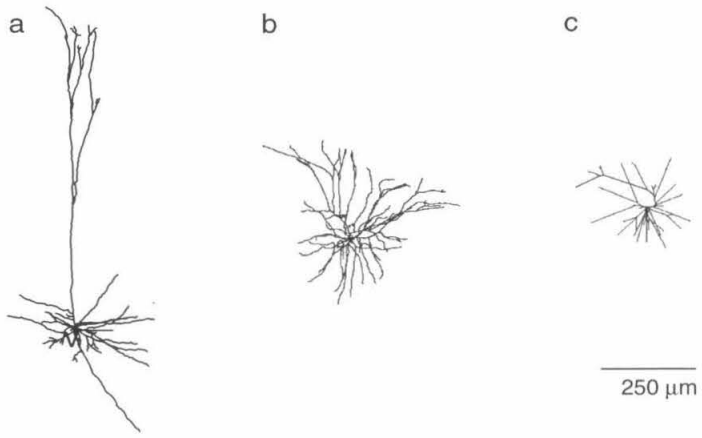

Figure 7.4: Morphology of model neurons
Digital reconstructions of dendritic arborizations of a Layer 5 pyramidal cell (a), a Layer 3 pyramidal cell (b), and a Layer 3 aspiny cell. The axons are not shown.

data (adding 0.83 μm^2 per linear μm of dendrite) (Bush & Sejnowski, 1993).

The specific membrane capacitance (C_m) was set to 0.75 μFcm^{-2} (except the myelinated axon segments, where C_m = 0.04 μFcm^{-2}). The specific membrane resistance (R_m) was 30 kΩ-cm^2 (except the axon node segments, where R_m = 50 Ω-cm^2). The specific axial resistance was 150 Ω-cm.

To simulate background activity, we added excitatory synapses distributed randomly on the dendrites, each of which was modeled by an alpha function conductance change with a peak amplitude of 0.5 nS and a time to peak of 1 ms (Bush & Sejnowski, 1993). Trains of the synaptic inputs were given according to a Poisson distribution.

7.3.2 Magnetic stimulation

Magnetic stimulation was simulated by injecting currents into the compartmental model based on the theory developed above. To determine the amount of injected current, the induced axial current has to be identified for the ends of the segment from which a single compartment is created, as well as for the neuronal terminals and the branching points. The axial current depends on the induced electric field, the fiber orientation, and the axial resistance at the point of interest.

We calculated the electric field due to magnetic induction using the method described in Chapter 6. The stimulator and coil parameters were the same as those used in the illustrations (Figure 6.1 and 6.2), except that the charged voltage was varied to change the amplitude of the electric field (the geometry and the time course were unchanged). The neuron model was assumed to be placed 1.5 cm below the coil surface. We also used spatially uniform electric fields with the same time course. They yielded similar results since the induced electric field from the coil (diameter, 7 cm) was nearly uniform for cortical neurons of a much smaller size (on the order of 100 μm).

Since the above neuron model assumes a constant specific axial resistance and cylindrical structure, the axial resistance was determined only by the diameter of the fiber. Each neural branch was divided into compartments of equal length, disregarding the points given in the reconstruction data. Hence, the fiber orientation and the diameter at the points of interest were obtained by linear interpolation of the discrete data.

We did not incorporate transmembrane currents at dendritic spines, as their geometry was not available in the reconstruction data. The contribution of the spines are, however, estimated to be small, because the transmembrane currents between the root and terminal of each spine, which are very closely spaced, are likely to cancel out. The axon was modeled as a straight cable, thus transmembrane currents at axonal bends and arborizations were not included in this model.

Chapter 8 Biophysical simulation and psychophysical implications

8.1 Excitation and inhibition by a magnetic pulse

Using the model developed in the previous chapter, we first investigate the basic effects of a magnetic pulse on resting and firing neurons. Firing neurons are of our interest since our psychophysical results suggested interactions of TMS with ongoing neural activity.

Figure 8.1 shows the time course of the membrane potential at the soma of the Layer 5 pyramidal neuron model with a magnetic pulse only (a), with background firing (b), or with both the magnetic pulse and the background firing (c). The induced electric field was spatially uniform (direction, from the soma to the apical dendrites), and the peak amplitude was set to 500 V/m which is comparable to the intensity used in TMS studies. The background firing was produced by 300 excitatory synapses randomly distributed on the dendrites (Bush & Sejnowski, 1993).

In the resting neuron, the magnetic pulse induced a single action potential (Figure 8.1a), while in the firing neuron, it led to a burst (a train of action potentials within 5-50 ms) followed by a long silent period, or inhibition of the background firing (c). The bursting behavior was observed in the resting neuron only when it was stimulated with much higher electric field intensity. Other morphological types of neuron models also showed similar effects, though with different thresholds: an action potential or burst was observed with a magnetic pulse, and bursting behavior was likely to be induced in firing neurons.

8.1.1 Biophysical mechanisms

The analysis of the channel currents revealed that the excitation (action potential and burst) was associated with the currents through high-threshold Ca^{2+} channels in the dendrites. During the excitation at the soma, Ca^{2+} channels were open in the dendrites producing a Ca^{2+} spike. This mechanism was confirmed by removing Ca^{2+} channels, whereupon the excitation was eliminated.

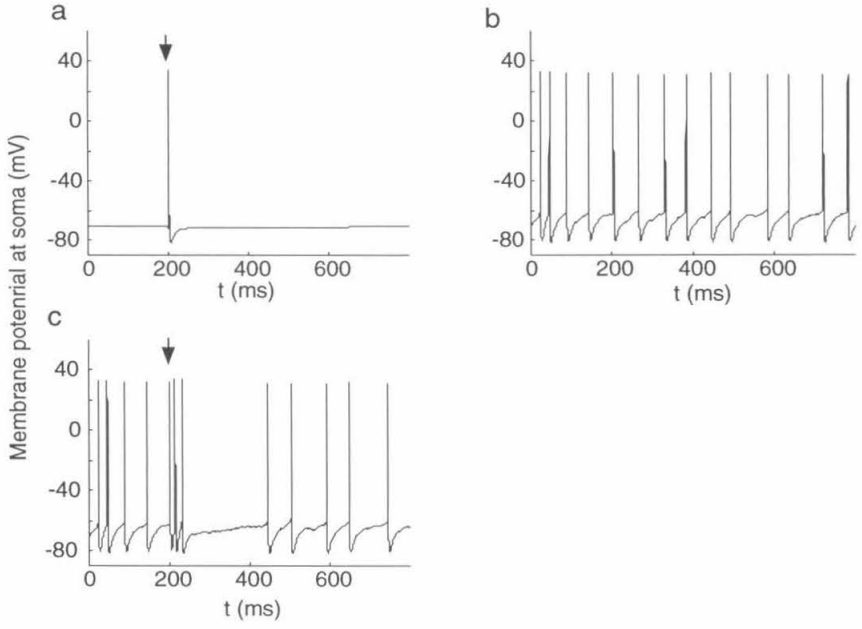

Figure 8.1: Excitation and inhibition by a magnetic pulse
The Layer 5 pyramidal cell was stimulated by a magnetic pulse only (a), by synaptic inputs (b), or by both the magnetic pulse and the synaptic inputs (c). The membrane potentials at the soma are plotted. The arrows indicate the timing of the magnetic pulse (duration, 1 ms).

The silent period observed in the firing neuron was due to the opening of Ca^{2+}-dependent K^+ channels in the dendrites and the soma. It was triggered by the calcium inflow due to the opening of Ca^{2+} channels. The activation of Ca^{2+}-dependent K^+ channels was also observed after the action potential in the resting neurons, though for a shorter period. Confirming this, the removal of Ca^{2+}-dependent K^+ channels eliminated the silent period, while the excitation remained the same.

The same magnetic stimulation caused more prominent effects in the firing neurons than in the resting neurons, presumably because the background synaptic inputs clamped the dendrites near the threshold for Ca^{2+} channels. It may also be possible that the backpropagation of an action potential from the soma coincided with positive current inputs due to magnetic stimulation in the dendrites, producing powerful Ca^{2+} spikes (Larkum *et al.*, 1999).

To further validate this mechanism for the excitation and inhibition, we need more detailed information as to the distribution of Ca^{2+} channels and their electrophysiological properties in neocortical neurons (Stafstrom *et al.*, 1985; Reuveni *et al.*, 1993; Kim & Connors, 1993; Stuart & Sakmann, 1994; Yuste *et al.*, 1994; Hirsch *et al.*, 1995). Also, it would be interesting to characterize the effect of the positive and negative current inputs given simultaneously at numerous sites as is the case of magnetic stimulation. Such stimulation may have unique effects in triggering Ca^{2+} spikes.

8.1.2 Relation to perceptual and behavioral effects of TMS

The simulation results demonstrated intriguing characteristics pertinent to basic perceptual and behavioral effects of TMS. First, the substantially long inhibition of neural activity (> 100 ms) in the model can explain the inhibitory effects of TMS on visual perception, which have a comparable time course (Chapter 3). Such long dynamics can not be produced in axonal models containing only Na^+ and fast K^+ channels. Note also that the profile in Figure 8.1c is qualitatively similar to the EMG recording showing muscle activity under voluntary contraction (Figure 6.5), starting with brief excitation and followed by a long inhibitory period.

The initial excitation may not be reflected in visual perception under single-pulse TMS, which typically causes suppression of perception, because the excitation by a single magnetic pulse is too brief to exceed the threshold for conscious perception (Amassian *et al.*,

1998). Paired-pulse TMS, which can generate phosphenes (Chapter 5), may cause prolonged excitation in the neurons leading to positive conscious percept. It would also be interesting to study how the time course of excitation and inhibition observed in the neuron model is reflected in that of positive and negative perceptual effects.

The simulation demonstrated higher sensitivity of firing neurons to magnetic stimulation as compared to resting neurons. This is consistent with the findings that the effects of TMS on the motor cortex are largely enhanced when it is applied during motor tasks (Rothwell *et al.*, 1991). It may also be related to the effective suppression of transient aspects of visual perception, since cortical neurons are known to respond more vigorously to transient visual inputs than to sustained ones (Chapter 5).

Since Ca^{2+}-dependent K^+ channels are involved in neural adaptation (Ohzawa *et al.*, 1985), the hyperpolarization due to their opening may underlie the similarity between TMS-induced scotomas and afterimages (Chapter 4). Also, the dendritic Ca^{2+} influx, which is known to lead to persistent change in synaptic function (Ghosh & Greenberg, 1995), may be related to TMS-induced long-term effects on cognitive performance, and mood in depression patients (Kosslyn *et al.*, 1999; Pascual-Leone *et al.*, 1996). These hypotheses may be tested by combining TMS and a dose of drugs that block calcium-dependent channels in the human brain (Ziemann *et al.*, 1996).

8.2 Directional selectivity for excitation

Since cortical neurons generally have an asymmetric arborization, the pattern of the trans-membrane currents due to magnetic stimulation can vary substantially by changing the direction of the applied electric field. Figure 8.2 demonstrates the effect of the direction of the electric field on the Layer 5 pyramidal neuron model, which was stimulated by a uniform electric field (peak amplitude, 500 V/m) in four different directions. To focus on the effect of dendritic structure, the direction of the axon was kept constant relative to the direction of the electric field.

As shown, the neuron was activated only by the direction $\mathbf{E_{A1}}$ (from the soma to the apical dendrites). For the other directions, even subthreshold fluctuations were quite small at the soma, though more fluctuations were observed at the dendrites. The direction pointing from the soma toward the apical dendrites was effective, presumably because a

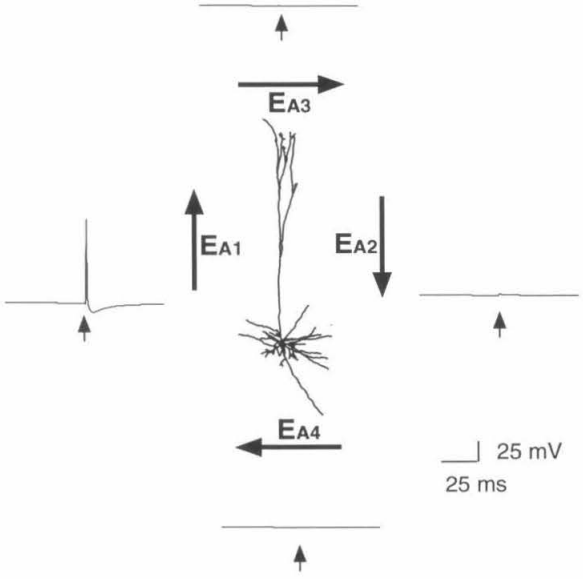

Figure 8.2: Directional selectivity for excitation
The Layer 5 pyramidal cell was stimulated by induced electric fields of four different directions ($\mathbf{E_{A1-4}}$). The membrane potential at the soma is plotted for each direction of the electric field. The small arrows indicate the timing of the stimulation.

large amount of transmembrane current is produced due to the decreasing diameter of the apical dendrites along the electric field, as well as their terminals, where the nearly parallel electric field effectively produce transmembrane currents.

The directional selectively shown in Figure 8.2 is consistent with the effect of the direction of the electric field on the perceived location of the scotoma (Chapter 3; see also Amassian, 1994), since the electric field toward the midline, which was shown to be effective for visual suppression, affects Layer 5 neurons in the medial bank of the visual cortex in the suppressed side, in the same manner as $\mathbf{E_{A1}}$. Other types of neurons as well as the effect of axonal structure, however, should be studied to determine the factors affecting the directional selectivity of TMS.

8.3 Neuronal size and excitability

In the previous chapter, we discussed the relationship between the size of the neuron and the effectiveness of stimulation. The steady state analysis of a straight cable under a uniform electric field suggested that long cables can be more effectively stimulated compared to short ones. To confirm it with a realistic neuron model, we change the length of each fiber in the Layer 5 pyramidal neuron, while keeping the diameters and the channel densities the same, and applying the same uniform electric field (peak amplitude, 500 V/m; direction, from the soma to the apical dendrites).

Figure 8.3 shows the membrane potential at the soma of the neuron models of 50% size (a), of the original size (b), and of 200% size (c). As predicted from the steady state analysis of a straight cable, the smaller model was not excited, while the larger model demonstrated excitation as the original one did.

Previous work by Nagarajan *et al.* (1993) suggested that short axonal cables are easier to stimulate with a magnetic pulse than long ones are, contrary to our results. However, they modeled the distribution of the electric field according to a coil of a 10 cm diameter, and used axonal cables of 1-8 cm length, which made axon length comparable to the spatial extent of the induced electric field. Therefore, their results reflect the effect of the geometry of the electric field unlike our results which were obtained with a uniform electric field. In addition, they manipulate the cable length within the range where the cancellation effect between the positive and negative inputs at the terminals was negligible (> 5 in electrotonic

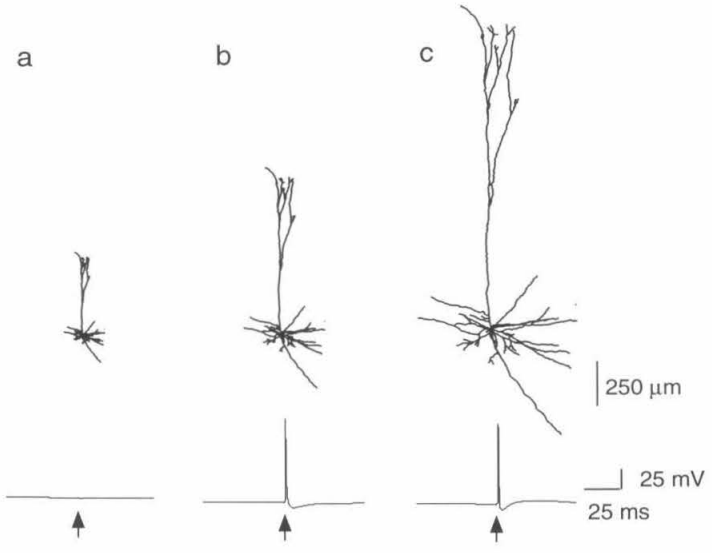

Figure 8.3: Neuronal size and excitability
The Layer 5 pyramidal cells of different sizes (a, 50%; b, the original size; c, 200%) were stimulated by a uniform electric field. The arrows indicate the timing of the stimulation.

length). For these reasons, their results do not apply to the analysis of cortical neurons with much smaller size, where the induced electric field can be regarded as nearly uniform, and the cancellation of the positive and negative inputs has to be taken into account.

Chapter 9 Summary and conclusions

TMS is potentially a powerful tool to study the relationship between human perception and neural activity, taking advantage of its direct interference with the neural electrical activity of conscious humans. In spite of numerous reports on the effects of TMS at the behavioral level, however, it has been difficult to produce a clearly perceptible phenomenon with TMS of sensory areas, especially using a single magnetic pulse. Also, the biophysical mechanism of magnetic stimulation in single cortical neurons has been poorly understood. In this thesis, we aimed to elucidate these fundamental issues of TMS, one at the psychophysical level and the other at the biophysical level.

In Part I (Psychophysics), we demonstrated perceptible effects of TMS of the human visual as results of the interactions with visual inputs:

P-1. The suppressive effect of TMS on the human visual cortex was made directly visible as a scotoma (a region lacking a pattern) in a flashed, large-field visual stimulus.

P-2. The spatial map and the time course of the TMS-induced scotoma were consistent with known anatomy and VEP data.

P-3. The location of the scotoma was dependent on the direction of the induced electric field.

P-4. The scotoma exhibited spatial distortion on visual patterns composed of luminance-defined gratings: the region appeared to be compressed along the stripes of the pattern.

P-5. Similar distortion of the scotoma was observed in illusory and luminance-defined contours/lines.

P-6. An afterimage projected on a grating pattern showed similar distortion as those in the TMS-induced scotoma.

P-7. The percept within the scotoma was shown to be a result of filling-in with the temporally adjacent visual feature.

P-8. Transient changes in visual stimuli, as opposed to brightness or spatial contrast, were shown to be effectively suppressed by TMS, using a small visual target presented within the scotoma region.

P-9. Paired-pulse TMS, which can generate phosphenes on a dark background, was shown

to modulate the brightness of transient and sustained visual stimuli in different manners.

These results generally indicate that visual perception induced by TMS reflects not just loss or addition of neural signals due to TMS, but the dynamic interactions with neural responses to visual inputs. Such interactions may occur not only within single neurons, but also via neuronal connections, as suggested by the spatial distortion effects of the scotoma. Hence, TMS of the human visual cortex offers a new clue to understand the dynamics of cortical circuitry, as opposed to mere cortical geometry, underlying our perceptual experience.

In Part II (Biophysics), we presented theory and simulations to model magnetic stimulation of single cortical neurons:

B-1. A biophysical theory was developed to simulate the effect of magnetic stimulation on arbitrary neuronal structure by means of current injection into a compartmental model.

B-2. Based on the theory, it was proved that the total injected current into a whole neuron of arbitrary structure is always zero.

B-3. A steady state analysis showed that, on the size scale of cortical neurons, long straight cables can be more effectively stimulated than short ones.

B-4. Computer simulation showed that a magnetic pulse can produce a long inhibitory period ($>$ 100 ms) following brief excitation in cortical neuron models with realistic structure and channels.

B-5. The analysis of channel currents in the neuron model revealed that calcium currents in the dendrites are critically involved in the excitation and inhibition of neural activity by magnetic stimulation.

B-6. Neuron models with background firing were more sensitive to magnetic stimulation than those at the resting state.

B-7. The effect of magnetic stimulation of a neuron model crucially depended on the direction of the applied electric field relative to the neuronal structure.

B-8. Large neuron models were more easily excited than small ones, consistent with the steady state analysis of a straight cable (B-3).

By incorporating realistic dendritic channels and complex structure, our model, unlike previous straight axonal models, exhibited behavior that can be linked to basic characteristics of the macroscopic effects of TMS including some of our psychophysical results, such as the substantially long suppression of visual perception (B-4, P-1, P-2), the enhancement

of the effect during transient visual inputs (B-6, P-8), and the directional selectivity of the stimulation (B-7, P-3).

Since our model is based on assumptions and simplifications concerning channel type, channel distribution, axonal geometry, extracellular space, etc., physiological studies to validate the model and more detailed modeling need to be conducted. Furthermore, to fully account for our psychophysical data, especially the spatial effects, we will have to extend to the single neuron model to network models that simulate cortical circuitry. Simulation of repetitive magnetic stimulation may also elucidate the biophysical mechanisms underlying the phosphenes due to paired-pulse TMS.

In conclusion, the perceptible effects of TMS and the cortical neuron model presented here provide solid foundations for the study of the relationship between human perception and neural activity. Further insights into the detailed causal relation would be obtained from the extension of our model to realistic cortical circuitry, and psychophysical experiments based on predictions of the biophysical model.

Bibliography

Amassian, V. E., Cracco, R. Q., Maccabee, P. J., Cracco, J. B., Rudell, A. & Eberle, L. (1989). Suppression of visual perception by magnetic coil stimulation of human occipital cortex. *Electroencephalography and clinical Neurophysiology* **74**, 458-462.

Amassian, V. E., Cracco, R. Q., Maccabee, P. J., Cracco, J. B., Rudell, A. & Eberle, L. (1993). Unmasking human visual perception with the magnetic coil and its relation to hemispheric asymmetry. *Brain Research* **605**, 312-316.

Amassian, V. E., Maccabee, P. J., Cracco, R. Q., Cracco, J. B., Somasundaram, M., Rothwell, P. J., Eberle, L., Henry, K. & Rudell, A. P. (1994). The polarity of the induced electric field influences magnetic coil inhibition of human visual cortex: Implications for the site of excitation. *Electroencephalography and clinical Neurophysiology* **93**, 21-26.

Amassian, V. E., Cracco, R. Q., Maccabee, P. J., Cracco, J. B., Rudell, A. P. & Eberle, L. (1998). Transcranial magnetic stimulation in study of the visual pathway. *Journal of Clinical Neurophysiology* **15**, 288-304.

Barker, A. T., Jalinous, R. & Freeston, I. L. (1985). Non-invasive magnetic stimulation of human motor cortex. *Lancet* **1**, 1106-1107.

Barker, A. T., Freeston, I. L., Jalinous, R. & Jarratt, J. A. (1987). Magnetic stimulation of the human brain and peripheral nervous system: An introduction and the results of an initial clinical evaluation. *Neurosurgery* **20**, 100-109.

Barlow, H. B., Kohn, H. L. & Walsh, E. G. (1947). Visual sensations aroused by magnetic fields. *American Journal of Physiology* **148**, 372-375.

Basser, P. J., Wijesinghe, R. S. & Roth, B. J. (1992). The activating function for magnetic stimulation derived from a three-dimensional volume conductor model. *IEEE Transactions on Biomedical Engineering* **39**, 1207-1210.

Beckers, G. & Hömberg, V. (1992). Cerebral visual motion blindness: Transitory akinetopia induces by transcranial magnetic stimulation of the human brain. *Proceedings of the Royal Society of London B* **249**, 173-178.

Bergman, P. S. (1955). Cerebral blindness. *Archives of Neurology* **78**, 568-584.

Bickford, R. G., Guidi, M., Fortesque, P. & Swenson, M. (1987). Magnetic stimulation of human peripheral nerve and brain: Response enhancement by combined magnetoelectrical technique. *Neurosurgery* **20**, 110-116.

Boroojerdi, B., Bushara, K. O., Corwell, B., Immisch, I., Battaglia, F., Muellbacher, W. & Cohen, L. G. (2000). Enhanced Excitability of the human visual cortex induced by short-term light deprivation. *Cerebral Cortex* **10**, 529-534.

Boroojerdi, B., Prager, A., Muellbacher, W. & Cohen, L. G. (2000). Reduction of human visual cortical excitability using 1-Hz transcranial magnetic stimulation. *Neurology* **54**, 1529-1531.

Breitmeyer, B. (1975). Simple reaction time as a measure of the temporal response properties of transient and sustained channels. *Vision Research* **15**, 1411-1412.

Breitmeyer, B. & Ganz, L. (1976). Implications of sustained and transient channels for theories of visual pattern masking, saccadic suppression, and information processing. *Psychological Review* **83**, 1-36.

Breitmeyer, B. G. (1984). *Visual Masking: An Integrative Approach.* Oxford: Oxford University Press.

Brindley, G. S. (1959). The discrimination of afterimages. *Journal of Physiology* **147**, 194-203.

Bush, P. C. & Sejnowski, T. J. (1993). Reduced compartmental models of neocortical pyramidal cells. *Journal of Neuroscience Methods* **46**, 159-166.

Chokroverty, S. (1989). *Magnetic Stimulation in Clinical Neurophysiology.* Boston, MA: Butterworth.

Cohen, D. (1985). Feasibility of a magnetic stimulator for the brain. In: Weinberg, Stroink & Katila (Eds.), *Biomagnetism: Applications and Theory*, (pp. 466-470). New York: Pergamon.

Cohen, L. G., Roth, B. J., Nilsson, J., Dang, N., Panizza, M., Bandinelli, S., Friauf, W. & Hallett, M. (1990). Effects of coil design on delivery of focal magnetic stimulation: Technical consideration. *Electroencephalography and clinical Neurophysiology* **75**, 350-357.

Cohen, L. G., Bandinelli, S., Sato, S., Kufta, C. & Hallett, M. (1991). Attenuation in detection of somatosensory stimuli by transcranial magnetic stimulation. *Electroencephalography and clinical Neurophysiology* **81**, 366-376.

Craik, K. J. M. (1940). Origin of visual after-images. *Nature* **145**, 512.

d'Arsonval, A. (1896). Dispositifs pour la mesure des courants alternatifs de toutes fréquences. *Comptes Rendus des Seances de la Societe de Biologie et de ses Filiales* **3**, 450-457.

Day, B. L., Rothwell, J. C., Thompson, P. D., Maertens de Noordhout, A., Nakashima, K., Shannon, K. & Marsden, C. D. (1989). Delay in the execution of voluntary movement by electrical or magnetic brain stimulation in intact man: Evidence for the storage of motor programs in the brain. *Brain* **112**, 649-663.

DeValois, R. L., Albrecht, D. G. & Thorell, L. G. (1982). Spatial frequency selectivity of cells in macaque visual cortex. *Vision Research* **22**, 545-559.

DeYoe, E. A., Carman, G. J., Bandettini, P., Glickman, S., Wieser, J., Cox, R., Miller, D. & Neitz, J. (1996). Mapping striate and extrastriate visual areas in human cerebral cortex. *Proceedings of the National Academy of Sciences of the United States of America* **93**, 2382-2386.

Douglas, R. J., Martin, K. A. & Whitteridge, D. (1991). An intracellular analysis of the visual responses of neurones in cat visual cortex. *Journal of Physiology (London)* **440**, 659-696.

Dunlap, K. (1911). Visual sensations from the alternating magnetic field. *Science* **33**, 68-71.

Durand, D., Ferguson, S. & Dalbasti, T. (1992). Effect of surface boundary charge on neuronal magnetic stimulation. *IEEE Transactions on Biomedical Engineering* **39**, 58-64.

Eaton, H. (1992). Electric field induced in a spherical volume conductor from arbitrary coils: Application to magnetic stimulation and MEG. *Medical & Biological Engineering & Computing* **30**, 433-440.

Epstein, C. M., Schwartzberg, D. G., Davey, K. R. & Sudderth, D. B. (1990). Localizing the site of magnetic stimulation. *Neurology* **40**, 666-670.

Epstein, C. M., Verson, R. & Zangaladze, A. (1996). Magnetic coil suppression of visual perception at an extracalcarine site. *Journal of Clinical Neurophysiology* **13**, 247-252.

Esselle, K. P. & Stuchly, M. A. (1994). Quasi-static electric field in a cylindrical volume conductor induced by external coils. *IEEE Transactions on Biomedical Engineering* **41**, 151-158.

Foster, K. R. & Schwan, H. P. (1989). Dielectric properties of tissues and biological materials: A critical review. *CRC Critical Reviews in Biomedical Engineering* **17**, 25-104.

Geddes, L. A. (1988). Optimal stimulus duration for extracranial cortical stimulation. *Neurosurgery* **20**, 94-99.

Gegenfurtner, K. R., Brown, J. E. & Rieger, J. (1997). Interpolation processes in the perception of real and illusory contours. *Perception* **26**, 1445-1458.

Ghosh, A. & Greenberg, M. E. (1995). Calcium signaling in neurons: Molecular mechanisms and cellular consequences. *Science* **268**, 239-247.

Gilbert, C. D., Hirsch, J. A. & Wiesel, T. N. (1990). Lateral interactions in the visual cortex. *Cold Spring Harbor Symposia on Quantitative Biology* **55**, 663-677.

Grosof, D. H., Shapley, R. M. & Hawken, M. J. (1993). Macaque V1 neurons can signal illusory contours. *Nature* **365**, 550-552.

Gutfreund, Y., Yarom, Y. & Segev, I. (1995). Subthreshold oscillations and resonant frequency in guinea-pig cortical neurons: Physiology and modelling. *Journal of Physiology* **483**, 621-640.

Hallett, M. (1995). Transcranial magnetic stimulation: Negative Effects. In: S. Fahn, M. Hallett, H. O. Lübers & C. D. Marsden (Eds.), *Negative Motor Phenomena*, (pp. 107-113). Philadelphia: Lippincott-Raven Publishers.

Hallett, M. (2000). Transcranial magnetic stimulation and the human brain. *Nature* **406**, 147-150.

Hallgren, R. (1973). Inductive nerve stimulation. *IEEE Transactions on Biomedical Engineering* **20**, 470-472.

Halliday, A. M. (1982). *Evoked Potentials in Clinical Testing.* Edinburg: Churchill Livingstone.

Hamill, O. P., Huguenard, J. R. & Prince, D. A. (1991). Patch-clamp studies of voltage-gated currents in identified neurons of the rat cerebral cortex. *Cerebral Cortex* **1**, 48-61.

Hines, M. (1993). NEURON: A program for simulation of nerve equations. In: F. Eeckman (Ed.), *Neural Systems: Analysis and Modeling*, (pp. 127-136). Boston, MA: Kluwer Academic Publishers.

Hirsch, J. A., Alonso, J. M. & Reid, R. C. (1995). Visually evoked calcium action potentials in cat striate cortex. *Nature* **378**, 612-616.

Horton, J. C. & Hoyt, W. F. (1991). Quadrantic visual field defects. *Brain* **114**, 1703-1718.

Hotson, J., Braun, D., Herzberg, W. & Boman, D. (1994). Transcranial magnetic stimulation of extrastriate cortex degrades human motion direction discrimination. *Vision Research* **34**, 2115-2123.

Ikeda, M. (1986). Temporal impulse response. *Vision Research* **26**, 1431-1440.

Inghilleri, M., Berardelli, A., Cruccu, G. & Manfredi, M. (1993). Silence period evoked by transcranial magnetic stimulation of the human cortex and cervicomedullary junction. *Journal of Physiology (London)* **466**, 521-534.

Jackson, J. D. (1975). *Classical Electrodynamics.* New York: John Wiley and Sons.

Jones, J. P. & Palmer, L. A. (1987). An evaluation of the two-dimensional Gabor filter model of simple receptive fields in cats striate cortex. *Journal of Neurophysiology* **58**, 1233-1258.

Kamitani, Y. & Shimojo, S. (1998). Visualizing suppression induced by transcranial magnetic stimulation: I. Localized loss of visibility in a large-field visual stimulus. *Investigative Ophthalmology and Visual Science* **39**, 3093.

Kamitani, Y., Shimojo, S. & Takahashi, Y. (1998). Visualizing suppression induced by transcranial magnetic stimulation: Backward Filling-in to suppressed region in visual pattern. *Society for Neuroscience Abstracts* **24**, 2096.

Kamitani, Y. & Shimojo, S. (1999a). Manifestation of scotomas created by transcranial magnetic stimulation of human visual cortex. *Nature Neuroscience* **2**, 767-771.

Kamitani, Y. & Shimojo, S. (1999b). Change suppression induced by transcranial magnetic stimulation. *Investigative Ophthalmology and Visual Science* **40**, 248.

Kamitani, Y., Bhalodia, V. M., Kubota, Y. & Shimojo, Y. (in press). A model of magnetic stimulation of Neocortical Neurons. *Neurocomputing.*

Kanizsa, G. (1979). *Organization in Vision: Essays on Gestalt Perception.* New York: Praeger.

Kapadia, M. K., Ito, M., Gilbert, C. D. & Westheimer, G. (1995). Improvement in visual sensitivity by changes in local context: Parallel studies in human observers and in V1 of alert monkeys. *Neuron* **15**, 843-856.

Kasai, T., Kawai, S., Kawanishi, M. & Yahagi, S. (1997). Evidence for facilitation of motor evoked potentials (MEPs) induced by motor imagery. *Brain Research* **744**, 147-150.

Kastner, S., Demmer, I. & Ziemann, U. (1998). Transient visual field defects induced by transcranial magnetic stimulation over occipital lobe. *Experimental Brain Research* **118**, 435-438.

Kim, H. G. & Connors, B. W. (1993). Apical dendrites of the neocortex: Correlation between sodium- and calcium-dependent spiking and pyramidal cell morphology. *Journal of Neuroscience* **13**, 5301-5311.

King, E. (1967). The nature of visual field deficits. *Brain* **90**, 647-668.

Koch, C. (1999). *Biophysics of Computation.* New York: Oxford University Press.

Kosslyn, S. M., Pascual-Leone, A., Felician, O., Camposano, S., Keenan, J. P., Thompson, W. L., Ganis, G., Sukel, K. E. & Alpert, N. M. (1999). The role of Area 17 in visual imagery: Convergent evidence from PET and rTMS. *Science* **284**, 167-170.

Krassowska, W. & Neu, J. C. (1994). Response of a single cell to an external electric field. *Biophysical Journal* **66**, 1768-1776.

Larkum, M. E., Zhu, J. J. & Sakmann, B. (1999). A new cellular mechanism for coupling inputs arriving at different cortical layers. *Nature* **398**, 338-341.

Larsson, J., Amunts, K., Gulyas, B., Malikovic, A., Zilles, K. & Roland, P. E. (1999). Neuronal correlates of real and illusory contour perception: Functional anatomy with PET. *European Journal of Neuroscience* **11**, 4024-4036.

Maccabee, P. J., Amassian, V. E., Eberle, L. P. & Cracco, R. Q. (1993). Magnetic coil stimulation of straight and bent amphibian and mammalian peripheral nerve in vitro: Locus of excitation. *Journal of Physiology* **460**, 201-219.

Maffei, L., Fiorentini, A. & Bisti, S. (1973). Neural correlates of perceptual adaptation to gratings. *Science* **182**, 1036-1039.

Magnusson, C. E. & Stevens, H. C. (1911). Visual sensations created by a magnetic field. *American Journal of Physiology* **29**, 124-136.

Mainen, Z. F., Joerges, J., Huguenard, J. R. & Sejnowski, T. J. (1995). A model of spike initiation in neocortical pyramidal neurons. *Neuron* **15**, 1427-1439.

Mainen, Z. F. & Sejnowski, T. J. (1996). Influence of dendritic structure on firing pattern in model neocortical neurons. *Nature* **382**, 363-366.

Marg, E. & Rudiak, D. (1994). Phosphenes induced by magnetic stimulation over the occipital brain: Description and probable site of stimulation. *Optometry and Visual Science* **71**, 301-311.

Mendola, J. D., Dale, A. M., Fischl, B., Liu, A. K. & Tootell, R. B. (1999). The representation of illusory and real contours in human cortical visual areas revealed by functional magnetic resonance imaging. *Journal of Neuroscience* **19**, 8560-8572.

Merton, P. A. & Morton, H. B. (1980). Stimulation of the cerebral cortex in the intact human subject. *Nature* **285**, 227.

Meyer, B. U., Diehl, R., Steinmetz, H., Britton, T. C. & Benecke, R. (1991). Magnetic stimuli applied over motor and visual cortex: Influence of coil position and field polarity on motor responses, phosphenes, and eye movements. *Electroencephalography and clinical Neurophysiology* **Supple. 43**, 121-134.

Mills, K. R. (1991). Magnetic brain stimulation: A tool to explore the action of the motor cortex on single human spinal motoneurones. *Trends in Neurosciences* **14**, 401-405.

Movshon, J. A. & Lennie, P. (1979). Pattern-selective adaptation in visual cortical neurons. *Nature* **278**, 850-852.

Nagarajan, S. S., Durand, D. M. & Warman, E. (1993). Effects of induced electric fields on finite neuronal structures: A simulation study. *IEEE Transactions on Biomedical Engineering* **40**, 1175-1188.

Nagarajan, S. S. & Durand, D. M. (1996). A generalized cable equation for magnetic stimulation of axons. *IEEE Transactions on Biomedical Engineering* **43**, 304-312.

Ohzawa, I., Sclar, G. & Freeman, R. D. (1985). Contrast gain control in the cat's visual system. *Journal of Neurophysiology* **54**, 651-667.

Parker, D. M. & Salzen, E. A. (1977). Latency changes in the human visual evoked response to sinusoidal gratings. *Vision Research* **17**, 1201-1204.

Paré, D., Lang, E. J. & Destexhe, A. (1998). Inhibitory control of somatodendritic interactions underlying action potentials in neocortical pyramidal neurons in vivo: An intracellular and computational study. *Neuroscience* **84**, 377-402.

Pascual-Leone, A., Gates, J. R. & Dhuna, A. (1991). Induction of speech arrest and counting errors with rapid-rate transcranial magnetic stimulation. *Neurology* **41**, 697-702.

Pascual-Leone, A., Brasil-Neto, J. P., Valls-Sole', J., Cohen, L. G. & Hallett, M. (1992). Simple reaction time to focal transcranial magnetic stimulation. *Brain* **115**, 109-122.

Pascual-Leone, A., Rubio, B., Pallardo, F. & Catala, M. D. (1996). Rapid-rate transcranial magnetic stimulation of left dorsolateral prefrontal cortex in drug-resistant depression. *Lancet* **348**, 233-237.

Pascual-Leone, A., Tarazona, F., Keenan, J., Tormos, J. M., Hamilton, R. & Catala, M. D. (1999). Transcranial magnetic stimulation and neuroplasticity. *Neuropsychologia* **37**, 207-217.

Pashler, H. (1988). Familiarity and visual change detection. *Perception and Psychophysics* **44**, 369-378.

Plonsey, R. & Heppner, D. (1967). Considerations of quasi-stationarity in electrophysiological systems. *Bulletin of Mathematical Biophysics* **29**, 657-664.

Polat, U. & Sagi, D. (1993). Lateral interaction between spatial channels: Suppression and facilitation revealed by lateral masking experiments. *Vision Research* **33**, 993-999.

Polat, U., Mizobe, K., Pettet, M. W., Kasamatsu, T. & Norcia, A. M. (1998). Collinear stimuli regulate visual responses depending on cell's contrast threshold. *Nature* **391**, 580-584.

Polson, M. J. R., Barker, A. T. & Freeston, I. L. (1982). Stimulation of nerve trunks with time-varying magnetic fields. *Medical & Biological Engineering* **20**, 243-244.

Rall, W. (1989). Cable theory for dendritic neurons. In: C. Koch & I. Segev (Eds.), *Methods in Neuronal Modeling*, (pp. 9-62). Cambridge, MA: MIT Press.

Rattay, F. (1986). Analysis of models for external stimulation of fibers. *IEEE Transactions on Biomedical Engineering* **BME-21**, 974-977.

Ren, C., Tarjan, P. P. & Popovič, D. B. (1995). A novel electric design for electromagnetic stimulation—The slinky coil. *IEEE Transactions on Biomedical Engineering* **42**, 918-925.

Rensink, R. A. (2000). Seeing, sensing, and scrutinizing. *Vision Research* **40**, 1469-1487.

Reuveni, I., Friedman, A., Amitai, Y. & Gutnick, M. J. (1993). Stepwise repolarization from Ca2+ plateaus in neocortical pyramidal cells: Evidence for nonhomogeneous distribution of HVA Ca2+ channels in dendrites. *Journal of Neuroscience* **13**, 4609-4621.

Ringach, D. L. & Shapley, R. (1996). Spatial and temporal properties of illusory contours and amodal boundary completion. *Vision Research* **36**, 3037-3050.

Roth, B. J. & Basser, P. J. (1990). A model of the stimulation of a nerve fiber by electromagnetic induction. *IEEE Transactions on Biomedical Engineering* **37**, 588-597.

Roth, B. J., Cohen, L. G. & Hallett, M. (1991). The electric field induced during magnetic stimulation. *Electroencephalography and clinical Neurophysiology* **Suppl. 43**, 268-278.

Roth, B. J., Saypol, J. M., Hallett, M. & Cohen, L. G. (1991). A theoretical calculation of the electric field in the cortex during magnetic stimulation. *Electroencephalography and clinical Neurophysiology* **81**, 47-56.

Roth, B. J. (1994). Mechanisms for electrical stimulation of excitable tissue. *Critical Reviews in Biomedical Engineering* **22**, 253-305.

Rothwell, J. C., Thompson, P. D., Day, B. L., Boyd, S. & Marsden, C. D. (1991). Stimulation of the human motor cortex through the scalp. *Experimental Physiology* **76**, 159-200.

Rothwell, J. C. (1993). Evoked potentials, magnetic stimulation studies, and event-related potentials. *Current Opinions in Neurology* **6**, 715-723.

Rovamo, J. & Virsu, V. (1979). An estimation and application of the human cortical magnification factor. *Experimental Brain Research* **37**, 495-510.

Rudiak, D. & Marg, E. (1994). Finding the depth of magnetic brain stimulation: A re-evaluation. *Electroencephalography and clinical Neurophysiology* **93**, 358-371.

Ruohonen, J., Panizza, M., Nilsson, J., Ravazzani, P., Grandori, F. & Tognola, G. (1996). Transverse-field activation mechanism in magnetic stimulation of peripheral nerves. *Electroencephalography and clinical Neurophysiology* **101**, 167-174.

Saypol, J. M., Roth, B. J., Cohen, L. G. & Hallett, M. (1991). A theoretical comparison of electric and magnetic stimulation of the brain. *Annals of Biomedical Engineering* **19**, 317-328.

Schiefer, U., Skalej, M., Kolb, M., Dietrich, T. J., Kolb, R., Braun, C. & Petersen, D. (1998). Lesion location influences perception of homonymous scotomata during flickering random dot pattern stimulation. *Vision Research* **38**, 1303-1312.

Schmolesky, M. T., Wang, Y., Hanes, D. P., Thompson, K. G., Leutgeb, S., Schall, J. D. & Leventhal, A. G. (1998). Signal timing across the macaque visual system. *Journal of Neurophysiology* **79**, 3272-3278.

Schwindt, P. C., Spain, W. J., Foehring, R. C., Stafstrom, C. E., Chubb, M. C. & Crill, W. E. (1988). Multiple potassium conductances and their functions in neurons from cat sensorimotor cortex in vitro. *Journal of Neurophysiology* **59**, 424-449.

Segev, I. & Burke, R. E. (1998). Compartmental models of complex neurons. In: C. Koch & I. Segev (Eds.), *Methods in Neuronal Modeling*, (pp. 93-136). Cambridge, MA: MIT Press.

Seghier, M., Dojat, M., Delon-Martin, C., Rubin, C., Warnking, J., Segebarth, C. & Bullier, J. (2000). Moving illusory contours activate primary visual cortex: An fMRI study. *Cerebral Cortex* **10**, 663-670.

Sereno, M. I., Dale, A. M., Reppas, J. B., Kwong, K. K., Belliveau, J. W., Brady, T. J., Rosen, B. R. & Tootell, R. B. H. (1995). Borders of multiple visual area in humans revealed by functional magnetic resonance imaging. *Science* **268**, 889-893.

Sheth, B. R., Sharma, J., Rao, S. C. & Sur, M. (1996). Orientation maps of subjective contours in visual cortex. *Science* **274**, 2110-2115.

Shimojo, S. & Kamitani, Y. (1998). Visualizing suppression induced by transcranial magnetic stimulation: II. Anisotropy of suppression in oriented patterns. *Investigative Ophthalmology and Visual Science* **39**, 3094.

Shimojo, S. & Kamitani, Y. (1999). Contour filling-in leads to compression effect in afterimage and TMS-induced suppression. *Investigative Ophthalmology and Visual Science* **40**, 4111.

Sloper, J. J. & Powell, T. P. (1978). Dendro-dendritic and reciprocal synapses in the primate motor cortex. *Proceedings of the Royal Society of London B* **203**, 23-38.

Smythe, W. R. (1968). *Static and Dynamic Electricity*. New York: McGraw-Hill.

Stafstrom, C. E., Schwindt, P. C., Chubb, M. C. & Crill, W. E. (1985). Properties of persistent sodium conductance and calcium conductance of layer V neurons from cat sensorimotor cortex in vitro. *Journal of Neurophysiology* **53**, 153-170.

Stensaas, S. S., Eddington, D. K. & Dobelle, W. H. (1974). The topography and variability of the primary visual cortex in man. *Journal of Neurosurgery* **40**, 747-755.

Storm, J. F. (1990). Potassium currents in hippocampal pyramidal cells. *Progress in Brain Research* **83**, 161-187.

Stuart, G. J. & Sakmann, B. (1994). Active propagation of somatic action potentials into neocortical pyramidal cell dendrites. *Nature* **367**, 69-72.

Sullivan, D. M., Borup, D. T. & Gandhi, O. P. (1987). Use of the finite-difference time-domain method in calculating EM absorption in human tissues. *IEEE Transactions on Biomedical Engineering* **34**, 148-157.

Tolhurst, D. J. (1975). Sustained and transient channels in human vision. *Vision Research* **15**, 1151-1155.

Ueno, S., Tashiro, T. & Harada, K. (1988). Localized stimulation of neural tissues in the brain by means of a paired configuration of time-varying magnetic fields. *Journal of Applied Physics* **64**, 5862-5864.

Ueno, S. (1994). *Biomagnetic Stimulation.* New York: Plenum Press.

Valls-Solé, J., Pascual-Leone, A., Wassermann, E. M. & Hallett, M. (1992). Human motor evoked responses to paired transcranial magnetic stimuli. *Electroencephalography and clinical Neurophysiology* **85**, 355-364.

von der Heydt, R., Peterhans, E. & Baumgartner, G. (1984). Illusory contours and cortical neuron responses. *Science* **224**, 1260-1262.

Walsh, P. (1946). Magnetic stimulation of the human retina. *Federation Proceedings* **5**, 109-110.

Wassermann, E. M. (1998). Risk and safety of repetitive transcranial magnetic stimulation: Report and suggested guidelines from the International Workshop on the Safety of

Repetitive Transcranial Stimulation, June 5-7, 1996. *Electroencephalography and clinical Neurophysiology* **108**, 1-16.

Weisstein, N. (1971). Metacontrast. In: D. Jameson & L. M. Hurvich (Eds.), *Handbook of Sensory Physiology*, (pp. 233-272). Berlin: Springer-Verlag.

Wilson, H. R. (1997). A neural model of foveal light adaptation and afterimage formation. *Visual Neuroscience* **14**, 403-423.

Wollner, D. A. & Catterall, W. A. (1986). Localization of sodium channels in axon hillocks and initial segments of retinal ganglion cells. *Proceedings of the National Academy of Sciences of the United States of America* **83**, 8424-8428.

Wu, D.-A., Kamitani, Y., Maeda, F. & Shimojo, S. (2001). Interaction of TMS -induced phosphenes and visual stimuli. *Vision ScienceS Society*, 198.

Yuste, R., Gutnick, M. J., Saar, D., Delaney, K. R. & Tank, D. W. (1994). Ca^{2+} accumulations in dendrites of neocortical pyramidal neurons: an apical band and evidence for two functional compartments. *Neuron* **13**, 23-43.

Zador, A. M., Agmon-Snir, H. & Segev, I. (1995). The morphoelectrotonic transform: A graphical approach to dendritic function. *Journal of Neuroscience* **15**, 1669-1682.

Ziemann, U., Lönnecker, S., Steinhoff, B. J. & Paulus, W. (1996). Effects of antiepileptic drugs on motor cortex excitability in humans: A transcranial magnetic stimulation study. *Annals of Neurology* **40**, 367-378.

Appendix

The cortical neuron model contained voltage- and Ca^{2+}-dependent ion channels (Mainen & Sejnowski, 1996). The current from each channel type was given by

$$I_{ion} = \bar{g}_{ion} a^x b (V - E_{ion}) \tag{1}$$

where $\bar{g}_{ion}$ is the local conductance density, a is an activation variable with x order kinetics, b is an optional inactivation variable, V is the local membrane potential, and E_{ion} is the reversal potential for the ionic species. The specific equations for the currents are detailed below.

The Na^+ current I_{Na} (Mainen *et al.*, 1995; Hamill *et al.*, 1991):

$$I_{Na} = \bar{g}_{Na} m^3 h (V - E_{Na}) \tag{2}$$

$$\frac{dm}{dt} = \alpha_m(V)(1 - m) - \beta_m(V)m \tag{3}$$

$$\frac{dh}{dt} = \alpha_h(V)(1 - h) - \beta_h(V)h \tag{4}$$

$$\alpha_m = \frac{0.182(V + 30)}{1 - \exp(-(V + 30)/9)} \tag{5}$$

$$\beta_m = \frac{-0.124(V + 30)}{1 - \exp((V + 30)/9)} \tag{6}$$

$$\alpha_h = \frac{0.024(V + 45)}{1 - \exp(-(V + 45)/5)} \tag{7}$$

$$\beta_h = \frac{-0.0091(V + 70)}{1 - \exp((V + 70)/5)} \tag{8}$$

$$\beta_\infty = \frac{1}{1 + \exp((V + 60)/6.2)} \tag{9}$$

where E_{Na} was 60 mV, and $\bar{g}_{Na}$ was 20 pSμm^{-2} in the dendrites, soma, and myelinated internodes, 30,000 pSμm^{-2} in the axon hillock, initial segment, and nodes of Ranvier.

The fast K^+ current I_{Kv} (Mainen *et al.*, 1995; Hamill *et al.*, 1991):

$$I_{Kv} = \bar{g}_{Kv} n (V - E_K) \tag{10}$$

$$\frac{dn}{dt} = \alpha_n(V)(1 - m) - \beta_n(V) n \tag{11}$$

$$\alpha_n = \frac{0.02(V - 25)}{1 - \exp(-(V - 25)/9)} \tag{12}$$

$$\beta_n = \frac{-0.002(V - 25)}{1 - \exp((V - 25)/9)} \tag{13}$$

where E_K was -90 mV, and $\bar{g}_{Kv}$ was 200 pSμm^{-2} in the soma and 2000 pSμm^{-2} in the axon.

The slow voltage-dependent K^+ current I_{Km} (Gutfreund *et al.*, 1995):

$$I_{Km} = \bar{g}_{Km} n (V - E_K) \tag{14}$$

$$\frac{dn}{dt} = \alpha_n(V)(1 - m) - \beta_n(V) n \tag{15}$$

$$\alpha_n = \frac{0.001(V + 30)}{1 - \exp(-(V + 30)/9)} \tag{16}$$

$$\beta_n = \frac{0.001(V + 30)}{1 - \exp((V + 30)/9)} \tag{17}$$

where $\bar{g}_{Km}$ was 0.1 pSμm^{-2}.

The high-threshold Ca^{2+} current I_{Ca} (Reuveni *et al.*, 1993):

$$I_{Ca} = \bar{g}_{Ca} m^2 h (V - E_{Ca}) \tag{18}$$

$$\frac{dm}{dt} = \alpha_n(V)(1 - m) - \beta_n(V) n \tag{19}$$

$$\frac{dh}{dt} = \alpha_h(V)(1 - h) - \beta_h(V) h \tag{20}$$

$$\alpha_m = \frac{0.055(V + 27)}{1 - \exp(-(V + 27)/3.8)} \tag{21}$$

$$\beta_m = 0.94 \exp(-(V + 75)/17) \tag{22}$$

$$\alpha_h = 4.54 \times 10^{-4} \exp(-(V + 13)/50) \tag{23}$$

$$\beta_h = \frac{0.0065}{1 + \exp(-(V + 15)/28)} \tag{24}$$

where E_{Ca} was 140 mV, and $\bar{g}_{Ca}$ was 0.3 pSμm^{-2}.

The Ca^{2+}-dependent K^+ current I_{KCa} (Sloper & Powell, 1978):

$$I_{KCa} = \bar{g}_{KCa} n (V - E_K) \tag{25}$$

$$\frac{dn}{dt} = \alpha_n(V)(1 - n) - \beta_n(V)n \tag{26}$$

$$\alpha_n = 0.01 \times [Ca^{2+}]_i \tag{27}$$

$$\beta_n = 0.02 \tag{28}$$

where $\bar{g}_{KCa}$ was 3 pSμm^{-2}. $[Ca^{2+}]_i$ is the intracellular calcium concentration. The dynamics of intracellular calcium in thin shell 0.1 μm beneath the membrane was given by

$$\frac{d[Ca^{2+}]_i}{dt} = (-10^5 I_{Ca}/2F) - ([Ca^{2+}]_i - [Ca^{2+}]_\infty)/\tau_{Ca} \tag{29}$$

where F is Faraday's constant (96,480 C/M), $[Ca^{2+}]_\infty$ was 0.1 μM, and τ_{Ca} was 200 ms.